Geochemistry Geophysics Geosystems G3
AN ELECTRONIC JOURNAL OF THE EARTH SCIENCES
Published by AGU and the Geochemical Society

*Article*
Volume 7, Number 4
13 April 2006
Q04007, doi:10.1029/2005GC001125
ISSN: 1525-2027

# Modeling open system metamorphic decarbonation of subducting slabs

**P. J. Gorman and D. M. Kerrick**
*Department of Geosciences, Pennsylvania State University, University Park, Pennsylvania 16802, USA (pgorman@geosc.psu.edu)*

**J. A. D. Connolly**
*Earth Sciences Department, Swiss Federal Institute of Technology, CH-8092 Zurich, Switzerland*

[1] Fluids derived from the devolatilization of subducting slabs play a critical role in the melting of the mantle wedge and global geochemical cycles. However, in spite of evidence for the existence and mobility of an aqueous fluid phase during subduction metamorphism, the effect of this fluid on decarbonation reactions in subducting lithologies remains largely unquantified. In this study we present results from thermodynamic modeling of metamorphic devolatilization of subducted lithologies for pressures up to 6 GPa using an approach which considers fluid fractionation from source lithologies and infiltration from subjacent lithologies. This open system approach in which fluid flow is an intrinsic component of the chemical model offers an alternative to closed system models of subduction zone decarbonation. In general, our models simulating pervasive fluid flow in subducting lithologies predict $CO_2$ fluxes measured from volcanic arcs more closely than models which assume purely channelized flow. Despite the enhanced effect of $H_2O$-rich fluid infiltration on subduction decarbonation, our results support the hypothesis that $CO_2$ is returned to the deep mantle at convergent margins, particularly in cool and intermediate subduction zones. Our results demonstrate that for most subduction zones, a significant proportion of the $CO_2$ derived from the slab is lost beneath the fore arc, and therefore $CO_2$ flux estimates based on measurements within the volcanic arc alone may significantly underestimate the slab-derived $CO_2$ flux for individual margins. Nevertheless, our predicted *global* slab-derived $CO_2$ flux from convergent margins of $0.35–3.12 \times 10^{12}$ mols $CO_2$/yr is in good agreement with previous estimates of global arc volcanic flux. Because our predicted global slab-derived $CO_2$ flux is significantly less than atmospheric $CO_2$ drawdown by chemical weathering, significant $CO_2$ emission from other geologic regimes (e.g., hot spots) would be required to balance the global carbon cycle.

**Components:** 12,408 words, 8 figures, 4 tables.

**Keywords:** carbon dioxide; devolatilization; metamorphism; subduction; thermodynamic modeling; volcanic degassing.

**Index Terms:** 8411 Volcanology: Thermodynamics (0766, 1011, 3611); 8413 Volcanology: Subduction zone processes (1031, 3060, 3613, 8170).

**Received** 25 August 2005; **Revised** 5 December 2005; **Accepted** 23 February 2006; **Published** 13 April 2006.

Gorman, P. J., D. M. Kerrick, and J. A. D. Connolly (2006), Modeling open system metamorphic decarbonation of subducting slabs, *Geochem. Geophys. Geosyst.*, *7*, Q04007, doi:10.1029/2005GC001125.

## 1. Introduction and Background

[2] Decarbonation of subducting slabs provides $CO_2$ for arc volcanism which is critical in determining both past and present atmospheric $CO_2$ concentrations [*Berner and Kothavala*, 2001; *Kerrick*, 2001]. Additionally, $CO_2$ retained within the slab beyond the volcanic arc is important to deep global carbon cycling [*Bebout*, 1995; *Zhu and*

*Ogasawara*, 2002] and mantle phase relations [*Keppler et al.*, 2003]. Globally, approximately 2.42 $km^2$/yr of oceanic crust is consumed at subduction zones, carrying with it an estimated $1.54 \times 10^{14}$ g $CO_2$ [*Jarrard*, 2003]. Estimates of the amount of $CO_2$ expelled by arc volcanism range from $0.04 \times 10^{12}$ mol/yr [*Snyder et al.*, 2001] to $3.1 \times 10^{12}$ mol/yr [*Sano and Williams*, 1996]. This wide range of values is indicative of not only the uncertainty in measuring $CO_2$ output from individual volcanic arcs, but also the potential errors in extrapolation of measurements at a few arcs to the output of arc volcanism globally. The release of $CO_2$ from the subducting slab at subarc depths is controlled by several factors that vary for different subduction zones (e.g., age of incoming plate, rate of plate convergence, and the distribution and concentration of volatiles in the incoming slab). In spite of these complications, most global carbon cycle models assume a simple linear relationship between subduction rate and the flux of $CO_2$ expelled from global arc volcanism [e.g., *Berner and Kothavala*, 2001]. Among other factors, this assumption ignores the roles of bulk-rock composition and thermal regime on subduction zone metamorphic decarbonation [*Kerrick*, 2001].

[3] In addition to exerting control over global carbon budgets, subduction zone metamorphic decarbonation is critically important to the generation of arc magmas. Though controversy exists regarding the melting of subducted lithologies as a potential source for arc volcanism [*Johnson and Plank*, 1999; *Kelemen et al.*, 2003], nearly all melting that occurs in subduction settings results from the presence of fluid. Consequently, the composition and the depth of release of fluid from slab sources in relation to the peridotite solidus in the mantle wedge are of central importance.

[4] The principle volatile components in subducting lithologies ($CO_2$ and $H_2O$) are respectively contained in carbonated and hydroxylated minerals within marine sediments, hydrothermally altered upper and lower crust, and serpentinized upper oceanic mantle. On the basis of the analysis of DSDP and ODP drill core data, *Plank and Langmuir* [1998] provide the most comprehensive data set available for the composition of sediments entering subduction zones. From the 26 suduction zones examined, *Plank and Langmuir* [1998] present an average bulk composition for the global subducting sediment (GLOSS) which is dominated by terrigenous material (76 wt%) and contains 3.01 wt% $CO_2$ and 7.29 wt% $H_2O$. Bulk chemical composition data for these subduction zones indicate a high variability of volatile content within the subducting sediment load worldwide (~0 to >20 wt.% for both $H_2O$ and $CO_2$). The data set for the oceanic crust is considerably more limited compared to that of the marine sediment lithologies. Although the upper extrusive section of the crust has been reasonably well sampled and analyzed, only a few ODP holes have penetrated significantly into the lower crust, and only one hole (Hole 504B) has sampled the mafic dike layer underlying the crustal extrusives. Sampling of the gabbro layer is equally limited. Nevertheless, estimates have been made for mineral-bound $H_2O$ and $CO_2$ within the oceanic crust on the basis of coulometric analysis, modal mineralogy, and seismic properties [*Staudigel et al.*, 1989; *Johnson and Semyan*, 1994; *Alt and Teagle*, 1999; *Carlson*, 2003; *Carlson and Miller*, 2004]. The oceanic upper mantle has not been penetrated by ocean drilling and has thus not been sampled in situ. Serpentinization of the slab mantle has been inferred, however, as an explanation for deep earthquakes in subduction zones and as an explanation for a low velocity region below the oceanic crust [*Peacock*, 2001; *Hacker et al.*, 2003; *Ranero et al.*, 2003]. However, the depth and extent of upper oceanic mantle serpentinization remain controversial [*Kerrick*, 2002]. The $CO_2$ content of the oceanic upper mantle is largely unknown.

[5] Although the abundance of volatile components in the subducting lithosphere remains somewhat unconstrained (particularly in the mafic crust), the participation of these volatiles in the generation of arc magmas is clearly established. The high temperatures required for dry-melting of mantle peridotite at the depths of arc magma formation implicate the involvement of a $H_2O$-rich fluid in mantle wedge anatexis. Indeed, observations of melt inclusions in volcanic rocks indicate that arc magmas may contain as much as 8 wt.% $H_2O$ [*Grove et al.*, 2002; *Wallace*, 2005]. Further, trace element systematics of arc volcanics strongly suggest a fluid contribution from the subducting slab. The elevated large-ion-lithopile/rare earth element ratio (LILE/REE) relative to depleted MORB, one of the key diagnostic features of arc magmas, is generally assumed to be the result of a slab-derived aqueous fluid component added to the mantle wedge magma source [*Tatsumi and Eggins*, 1995]. Additionally, the presence of the cosmogenic radionucleide $^{10}Be$ and the common existence of positive Sr anomalies in arc lavas are indicative of contributions from both sedimentary and oceanic

crustal sources, respectively [*Morris and Tera*, 1989; *Elliott*, 2004].

[6] Previous studies by *Kerrick and Connolly* [1998, 2001a, 2001b] found marked differences in the extent of devolatilization of subducted lithologies with respect to bulk composition and the thermal regimes of various subduction zones. On the basis of their closed system analysis, decarbonation at subarc depths was found to be negligible in most lithologies except metabasalts, and only along high temperature geotherms in the case of that lithology [*Kerrick and Connolly*, 2001b]. Although the protoliths considered by *Kerrick and Connolly* [1998, 2001a, 2001b] do not undergo extensive decarbonation, metabasalts and upper mantle serpentinites undergo considerable dehydration during subduction. Infiltration of $H_2O$-rich fluids into carbonate-bearing lithologies in equilibrium with an $H_2O$-$CO_2$ fluid mixture will reduce the activity of $CO_2$ by dilution and thus induce metamorphic decarbonation [e.g., *Rumble et al.*, 1982; *Ferry*, 1991]. The closed system assumption employed by *Kerrick and Connolly* [1998, 2001a, 2001b] does not permit quantification of the effect of externally derived fluid on decarbonation reactions. An alternative approach, potentially more useful for predicting arc $CO_2$ flux, is to allow fluid fractionation from source lithologies and infiltration of fluids from subjacent lithologies. *Connolly* [2005] explored a simple model for pervasive infiltration-driven decarbonation of subducted metabasalts and concluded that such models do not appreciably alter the conclusion reached with earlier closed system modeling that a significant amount of subducted carbonate persists beyond subarc depths. Here we expand on this general model by (1) considering the extremes of the range of P-T conditions realized in global subduction zones, (2) including the contribution from decarbonation of subducted sediments to slab-derived $CO_2$ flux, and (3) introducing a model to evaluate the effect of fluid channelization on subduction zone decarbonation.

[7] Several lines of evidence attest to the mobility of subduction zone fluids. First, there is general agreement that the trace element signatures of arc magmas indicate the contribution of a slab-derived fluid [*Elliott*, 2004]. Second, for a broad range of subduction zone geotherms, the breakdown of hydrous phases in subducting lithologies at subarc depths [*Kerrick and Connolly*, 1998, 2001a, 2001b] implies that fluids derived from dehydration of the subducting slab play a critical role in the melting of the mantle wedge and consequent arc volcanism. Third, several recent studies suggest that infiltration of fluids plays an important role in the metamorphism of subducting lithologies [*Becker et al.*, 2000; *Franz et al.*, 2001; *Sadofsky and Bebout*, 2001; *Romer et al.*, 2003; *John and Schenk*, 2003; *John et al.*, 2004].

[8] In this study thermodynamic modeling was used to quantify the effects of fluid infiltration and fractionation on decarbonation reactions in subducting lithologies. By tracking the loss of $CO_2$ from subducting slabs, we compared the flux predicted from our models to measurements of $CO_2$ flux from volcanic arcs. Further, by considering extreme subduction thermal regimes and lithospheric hydration states, we evaluate the nature of fluid-rock interaction in the subducting lithosphere and constrain the global flux of $CO_2$ from convergent margins.

## 2. Modeling Approach

### 2.1. Computational Strategy

[9] As in previous studies of subduction zone decarbonation [*Kerrick and Connolly*, 1998, 2001a, 2001b; *Connolly*, 2005] we employ free energy minimization [*Connolly*, 1990] to compute high-pressure phase equilibria for subduction zone protoliths. For mineral end-member compositions, the thermodynamic data required for our calculations are taken from the database of *Holland and Powell* [1998] (revised 2002). The thermodynamic behavior of $H_2O$-$CO_2$ fluids are modeled using the CORK equation of state [*Holland and Powell*, 1991]. Biotite, chlorite, orthopyroxene, talc, phengite, dolomite, magnesite, garnet, olivine, and phase-A were treated as solutions using thermodynamic models summarized by *Connolly* [2005].

### 2.2. Fluid Flow Considerations

[10] Although the precise nature of fluid flow in deeply subducted crust remains enigmatic (for a recent review, see *Ague* [2003]), cogent evidence for a slab-derived component to arc volcanism attests to a significant vertical component to flow. Also, on the basis of systematic variation of cold spring water chemistry in the Mariana fore arc, *Mottl et al.* [2004] inferred that fluids evolved from the subducting slab follow near-vertical pathways. Thus our modeling of open system behavior assumed simple upward flow of fluids generated by devolatilization. By specifying flow in an upward direction, fluids evolved during devolatilization of

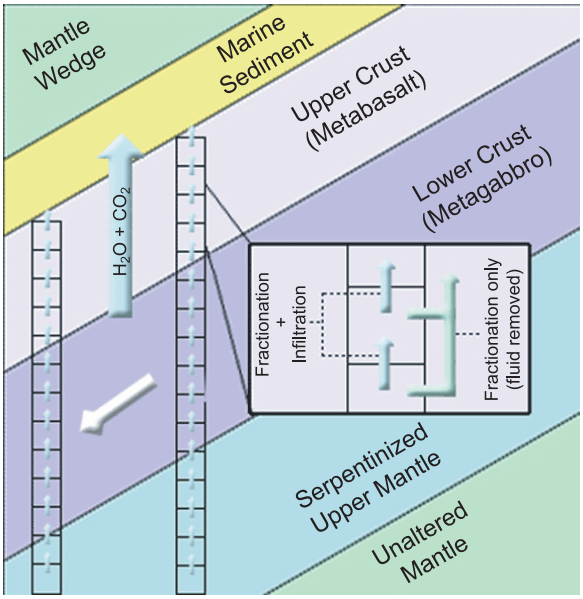


**Figure 1.** Schematic depiction of modeling approach. Subduction was modeled by the stepwise variation of pressure and temperature along a path prescribed by a selected thermal model. The slab was divided into a 2 km upper crust with an average oceanic metabasalt composition [*Staudigel et al.*, 1989], a 5 km lower crustal section of gabbroic composition [*Behn and Kelemen*, 2003] with 1% $H_2O$ due to hydrothermal alteration [*Carlson*, 2003], and an upper mantle section ranging in thickness from 0 to 20 km having a primitive mantle composition [*Hart and Zindler*, 1986] with the addition of 4 wt% $H_2O$ as a liberal estimate of upper mantle serpentinization [*Ranero et al.*, 2003; *Carlson and Miller*, 2003; *Connolly*, 2005]. Compositions of the marine sedimentary lithologies were taken from *Plank and Langmuir* [1998]. The slab was discretized into boxes of equal height, and for each step along the subduction path, PERPLEX was used to compute the equilibrium mineralogy within each box from the base of the slab upward. For open system models, fluid was removed from the bulk composition of the box from which it evolved. For infiltration models, the evolved fluid was added to the bulk composition of the overlying box [*Connolly*, 2005], whereas for fractionation-only models (distillation), the fluid was removed from the system (inset).

a given lithology will directly impact the phase equilibria and hence devolatilization of the overlying lithologies. Another important consideration in modeling fluid flow is the mechanism of fluid propagation. Fluid propagation through rock is considered to be "pervasive" or "channelized," or some combination of the two. Pervasive flow occurs along grain boundaries or microfractures whereas channelized flow occurs along larger cracks or fractures. When fluid flow is channelized, fluid-rock interaction is limited to channel walls as fluid rapidly escapes the system, whereas for pervasive flow fluid interacts uniformly with the entire rock body it passes through. As channelized flow and pervasive flow represent end-members in the range of possible fluid-rock interaction, we employ two types of open system models: (1) evolved fluid is removed immediately from the system (simulating fluid channelization) and (2) evolved fluid migrates to superjacent lithologies by pervasive flow (infiltration) (Figure 1). To differentiate these models hereafter, we refer to the former as a distillation model and the latter as an infiltration model.

## 2.3. Slab Composition Modeling

[11] Compositional variation was treated by considering a section of upper oceanic lithosphere that is divided into three main lithologic layers of prescribed thickness: upper oceanic mantle, oceanic crustal mafics, and marine sediments. The oceanic crustal layer is further divided into a more hydrated/carbonated upper crust and a comparatively volatile-poor lower crust. For modeling the entire stack is discretized at 100 m intervals (Figure 1). Having defined bulk rock composition, temperature and pressure, and the mobile fluid behavior in a lithospheric section, we calculate the stable phases in each box of the stack. Starting with the lowest box in the stack, the stable phase assemblage was determined and any fluid evolved was then added to the composition of the overlying box (Figure 1). Computations were performed sequentially until the topmost box of the section was reached, at which time the evolved fluid from the uppermost box was expelled from the top of the stack and removed from the system. Having completed the calculation for every box in the stack, the entire section was incrementally moved down the subduction path (Figure 1) and the devolatilization process was repeated.

## 2.4. Thermal Conditions

[12] Given the importance of the temperature and pressure profile along a subduction path in determining the depth and extent of devolatilization [*Kerrick and Connolly*, 1998, 2001a, 2001b; *Hacker et al.*, 2003], we have considered the extreme conditions of rapid subduction of mature lithosphere (cool subduction) versus slow subduction of young lithosphere (warm subduction). For thermal regimes we have adopted that of Honshu for cool subduction (91 mm/yr, 130 Ma) and Cascadia for warm sub-

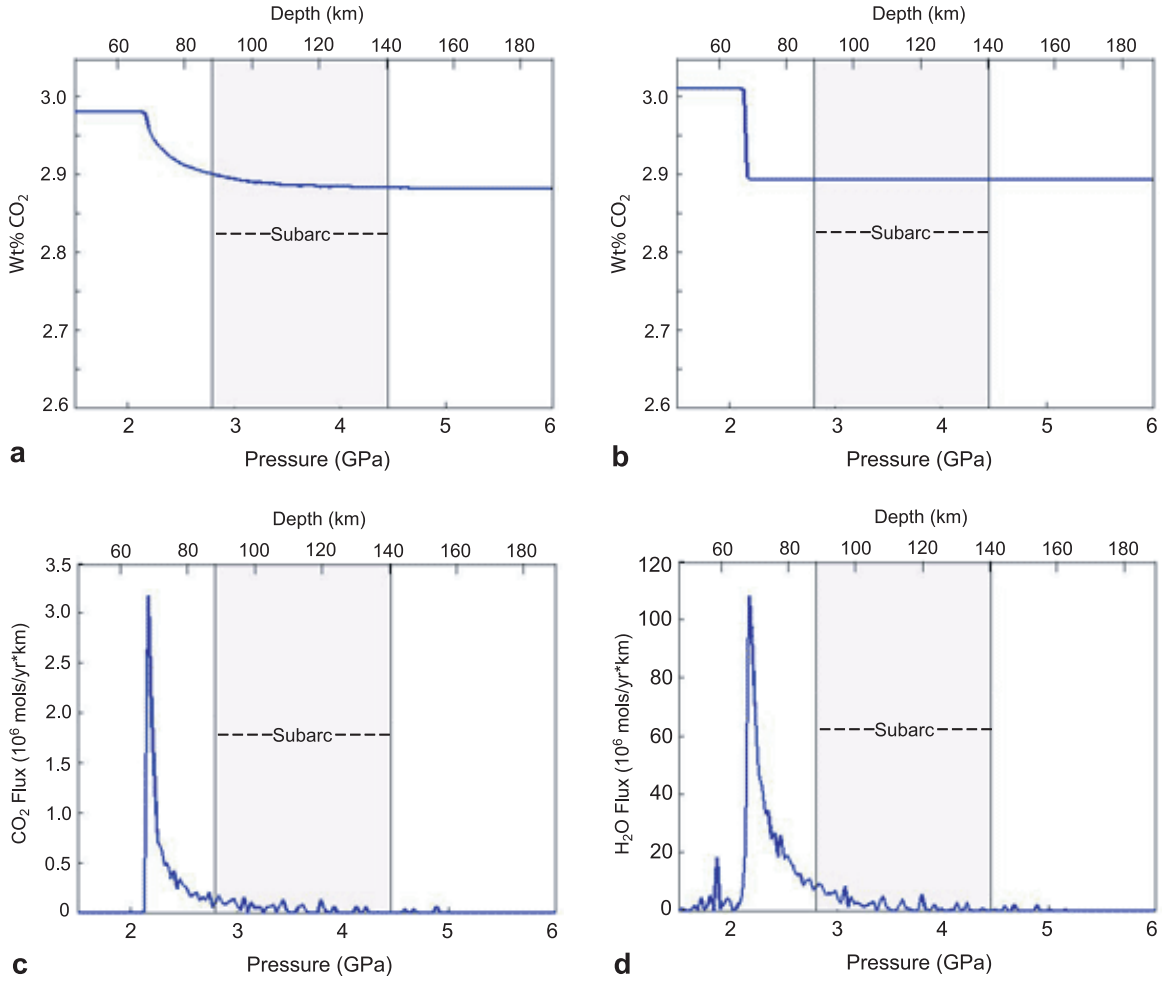


**Figure 2.** Results of distillation decarbonation models for cool subduction (e.g., Honshu). Subarc depths taken from *Tatsumi and Eggins* [1995]. (a) Decarbonation trend for metabasalt lithology. (b) Decarbonation trend for GLOSS. (c) $CO_2$ flux from the top of the subducting slab. (d) $H_2O$ flux from the top of the slab.

duction (45 mm/yr, 15 Ma). In addition to plate age and convergence rate, mantle wedge rheology exerts significant control over slab interface temperatures. We utilized thermal models of Honshu and Cascadia from *van Keken et al.* [2002] which employ temperature- and stress-dependent wedge viscosity. These models generally yield higher slab temperatures compared to earlier models assuming an isoviscous mantle wedge rheology [e.g., *Peacock and Wang*, 1999].

## 3. Results

[13] In this section, we present the results of our decarbonation models for cool and warm subduction. Because the models presented in this section are not intended to represent the devolatilization trends of specific subduction zones, we assume globally averaged compositions for subducting lithologies. For the marine sediment lithology considered here, we use a 500 m section having the GLOSS composition of *Plank and Langmuir* [1998] which contains 3.01 wt.% $CO_2$ and 7.29 wt.% $H_2O$. For the oceanic crust, we employ an average mid-ocean ridge (MOR) metabasalt composition [*Staudigel et al.*, 1989] containing 2.95 wt.% $CO_2$ and 2.68 wt.% $H_2O$. The compositions of the lower crust and mantle are as described in section 2.

### 3.1. Distillation Models

[14] Results of the distillation fluid models for cool subduction are shown in Figure 2. For the metabasalt lithology considered in this study, ~97% of the original mineral-bound $CO_2$ is retained beyond 200 km for cool subduction (Figure 2a). Most of the $CO_2$ lost from this lithology is expelled in a discrete pulse under the fore arc. This pulse is

**Table 1.** Summary of $CO_2$ Flux for Fluid Distillation Models

| | Pressure of Max $CO_2$ Pulse, GPa | Max $CO_2$ Pulse Flux, $10^6$mols/yr·km | Fore Arc $CO_2$ Flux, $10^6$mols/yr·km | Subarc $CO_2$ Flux, $10^6$mols/yr·km |
|---|---|---|---|---|
| Cool subduction | 2.2 | 3.2 | 11.9 | 2.0 |
| Warm subduction | 2.4–2.6 | 7.24 | 47.9 | 0 |

coincident with the intersection of the slab with the nose of the mantle wedge. Similar to the metabasalt decarbonation trend, the loss of $CO_2$ from the sediment lithology (GLOSS) is limited to ~4% of original $CO_2$, with the remainder subducted into the deeper mantle (Figure 2b). The expulsion of $CO_2$ from this lithology occurs entirely within the fore arc. The combined flux of $CO_2$ from the metabasalt and GLOSS lithologies is shown in Figure 2c and summarized in Table 1. As can be predicted by the decarbonation trends from Figures 2a and 2b, the majority of $CO_2$ flux occurs in the fore arc with the maximum pulse of $CO_2$ being coincident with the sharp drop off in carbonate content of the metasedimentary layer at 2.2 GPa. $CO_2$ production at this pressure is largely the result of dolomite decomposition in the presence of $H_2O$ generated by lawsonite breakdown. The $CO_2$ flux approaches zero beyond this pressure, with the total flux in the subarc being less than one-fifth of the fore-arc flux. In spite of the large flux of $CO_2$ under the fore arc, the composition of the evolved fluid is very nearly pure $H_2O$ ($X_{CO2} < 0.03$) at all depths due to the large flux of $H_2O$ that is coincident with major pulses of $CO_2$ (Figure 2d).

[15] For warm subduction, metabasalts still only lose a small percentage of their original $CO_2$ (~4%) (Figure 3a). However, in contrast to cool subduction, all of the $CO_2$ from this lithology is expelled in the fore arc. For GLOSS, ~93% of original bound $CO_2$ is lost at fore-arc depths, with no further release occurring at or beyond subarc depths (Figure 3b). The combined flux of $CO_2$ from the metabasalt and GLOSS lithologies under warm subduction is shown in Figure 3c and summarized in Table 1. Two distinct peaks occur in the $CO_2$ flux trend. The first, centered at ~2.25 GPa, is the result of the decomposition of dolomite within both the metabasalt and GLOSS lithologies in the presence of $H_2O$ generated from the breakdown of lawsonite. The second peak results from further dolomite decomposition within the GLOSS lithology. In contrast to cool subduction, the composition of the fluid that is expelled from the top of the subducting slab has $X_{CO2}$ up to 0.8, depending on the degree of lithospheric hydration. Although subjacently derived fluid does not drive decarbonation in our distillation models, the fluid evolved at the top of the slab is the summation of fluid lost from all boxes in the stack. For cases where there is no water in the mantle or lower crust, the $CO_2$ mole fraction of the evolved fluid is greatest.

## 3.2. Pervasive Infiltration Models

[16] For open system models allowing for pervasive fluid infiltration, decarbonation is dependent on both the P-T path and the extent of hydration of the lithosphere. The results of the infiltration fluid models for cool subduction are shown in Figure 4. For all degrees of subjacent lithospheric hydration, metabasalt loses approximately 15% of original carbonate beneath the fore arc for cool subduction (Figure 4a). For models with no lower crust or mantle water sources, only ~4% of original carbonate is lost in the subarc, with the remainder being subducted to depths >200 km. For models that include hydration of the lower crust (with or without accompanying upper mantle serpentinization), ~9% of the original carbonate is lost at subarc depths, with progressive $CO_2$ loss occurring beyond the subarc. For the marine sediment lithology (GLOSS) under cool subduction conditions, ~90% of original $CO_2$ is lost during infiltration-driven decarbonation under the fore arc, irrespective of the extent of lithospheric hydration (Figure 4b). For models with no additional subjacent water sources, ~8% of original carbonate is lost in the subarc, with the remainder being subducted into the deeper mantle. For models that include hydration of the lower crust (with or without upper mantle hydration), all of the $CO_2$ that is not lost in the fore arc (~10%) is lost at subarc depths. Therefore none of the original $CO_2$ in the GLOSS layer is retained beyond the subarc. The combined flux of $CO_2$ from the metabasalt and GLOSS lithologies under cool subduction is shown in Figure 4d and summarized in Table 2. The maximum pulse of $CO_2$ from the top of the slab occurs under the fore arc at a pressure of ~2.25 GPa and corresponds to the infiltration of $H_2O$-rich fluid derived from the breakdown of lawsonite within the upper crust (metabasalt) and sedimentary layer. As the subducting slab is warmed

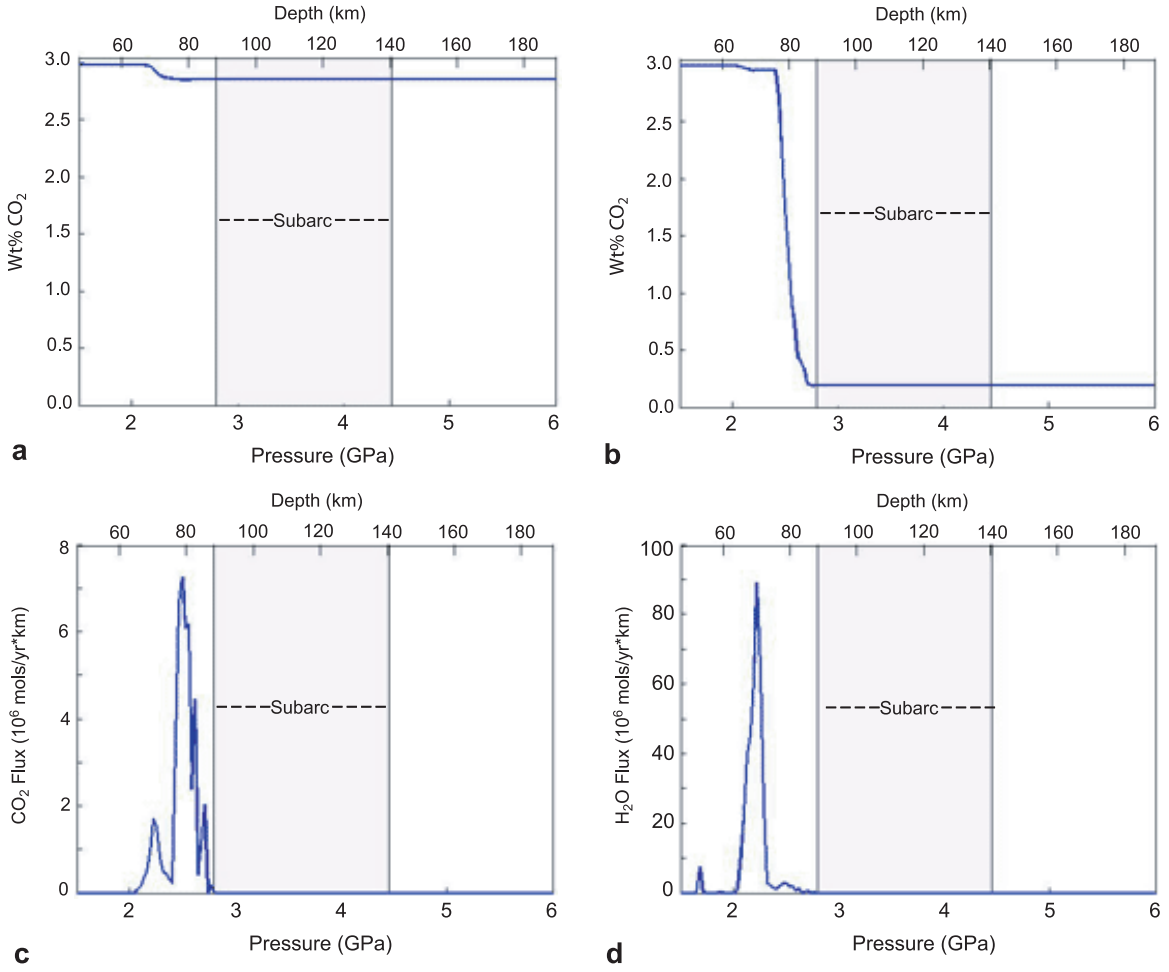


**Figure 3.** Results of distillation decarbonation models for warm subduction (e.g., Cascadia). (a) Decarbonation trend for metabasalt lithology. (b) Decarbonation trend for GLOSS. (c) $CO_2$ flux from the top of the subducting slab. (d) $H_2O$ flux from the top of the slab.

by the overlying mantle wedge, the decomposition of lawsonite and talc at increasingly lower levels in the crust continues to be a source of infiltrating fluid in the subarc. The total integrated $CO_2$ flux in the subarc is $\sim 20 \times 10^6$–$40 \times 10^6$ mols/yr per km of arc length, depending on the presence or absence of lower crustal hydration. Beyond the subarc, the breakdown of chlorite and antigorite within the hydrated upper mantle provide a fertile source of infiltrating $H_2O$-rich fluid to drive decarbonation. The composition of the fluid evolved from the top of the subducting slab under cool subduction varies between a nearly pure $H_2O$ fluid ($X_{CO2}$ $\sim$0.05) to a fluid with $X_{CO2}$ $\sim$0.2 (Figure 4c). The maximum $CO_2$ content of the fluid is achieved in the fore arc and decreases with increasing depth. The average $CO_2$ content of the evolved fluid is slightly higher for models without subjacent $H_2O$ sources, but still is constrained to the range $0.05 \leq X_{CO2} \leq 0.2$.

[17] For warm subduction, metabasalts lose approximately 13% of original carbonate beneath the fore arc for models with no additional subjacent water sources (Figure 5a). In this case, no additional $CO_2$ is evolved in the subarc. For models that include hydration of the lower crust (with or without accompanying upper mantle serpentinization), 100% of the original carbonate is lost at forearc depths. In all cases, no $CO_2$ is evolved at subarc depths. For the marine sediment lithology (GLOSS) under warm subduction conditions, $\sim$94% of original $CO_2$ is lost during infiltration-driven decarbonation in the fore arc, for models with no additional subjacent water sources (Figure 5b). The remaining 6% is retained beyond the subarc. For models that include hydration of the lower crust (with or without upper mantle hydration), all of the original $CO_2$ is lost in the fore arc. The combined flux of $CO_2$ from the metabasalt and GLOSS lithologies under cool subduction is shown

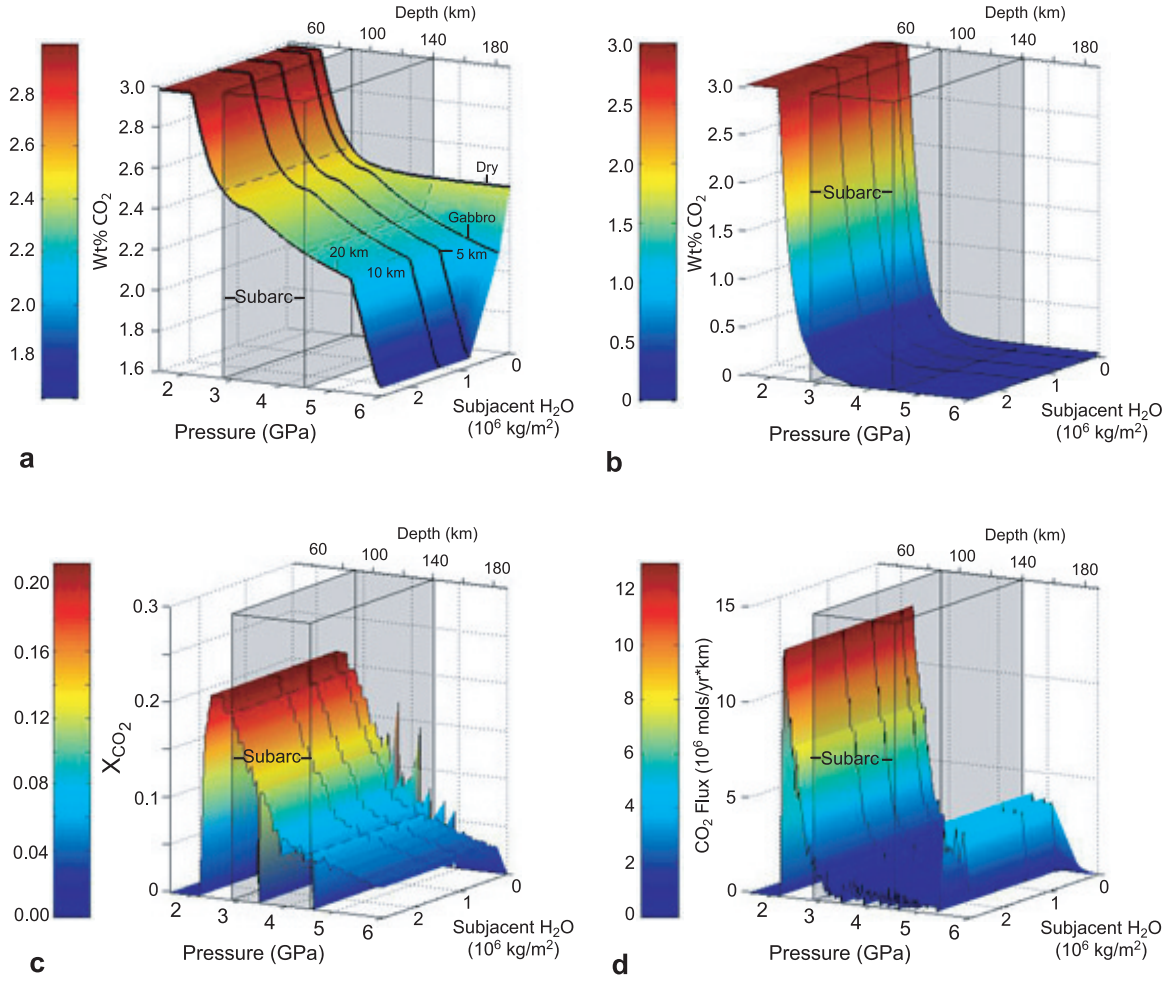


**Figure 4.** Results of infiltration decarbonation models for cool subduction. The axis labeled "Subjacent $H_2O$" indicates the amount of water in the subjacent lithosphere. Heavy lines in Figure 4a indicate amounts of subjacent $H_2O$ for specific model runs. Models including upper mantle hydration to 5, 10, and 20 km are labeled "5 km," "10 km," and "20 km," respectively. The "Gabbro" model includes a dry upper mantle and a hydrated lower crust (gabbro). The "Dry" model has no water subjacent to the upper crust. (a) Decarbonation trend for metabasalt lithology. (b) Decarbonation trend for GLOSS. (c) Composition of fluid evolved from the top of the subducting slab. (d) $CO_2$ flux from the top of the slab.

in Figure 5d and summarized in Table 2. The maximum pulse of $CO_2$ from the top of the slab occurs under the fore arc between 2.3 and 2.5 GPa and corresponds to the breakdown of lawsonite in the crust and sedimentary layer. The total integrated flux of $CO_2$ beneath the fore arc is variable, depending on the extent of lithospheric hydration. For models with no subjacent water sources, the total integrated flux is ~130 Mmols/yr/km arc length. For models involving a hydrated lower crust (with or without upper mantle serpentinization), the total integrated flux is ~444 Mmols/yr/km arc length. The composition of the fluid evolved from the top of the subducting slab beneath the fore arc varies

**Table 2.** Summary of $CO_2$ Flux for Pervasive Fluid Infiltration Models

| | Pressure of Max $CO_2$ Pulse, GPa | Max $CO_2$ Pulse Flux, $10^6$mols/yr·km | Fore Arc $CO_2$ Flux, $10^6$mols/yr·km | Subarc $CO_2$ Flux, $10^6$mols/yr·km |
|---|---|---|---|---|
| Cool subduction | 2.25 | 13 | 138 | 20–40 |
| Warm subduction | 2.3–2.5 | 70.6 | 130–444 | 0 |

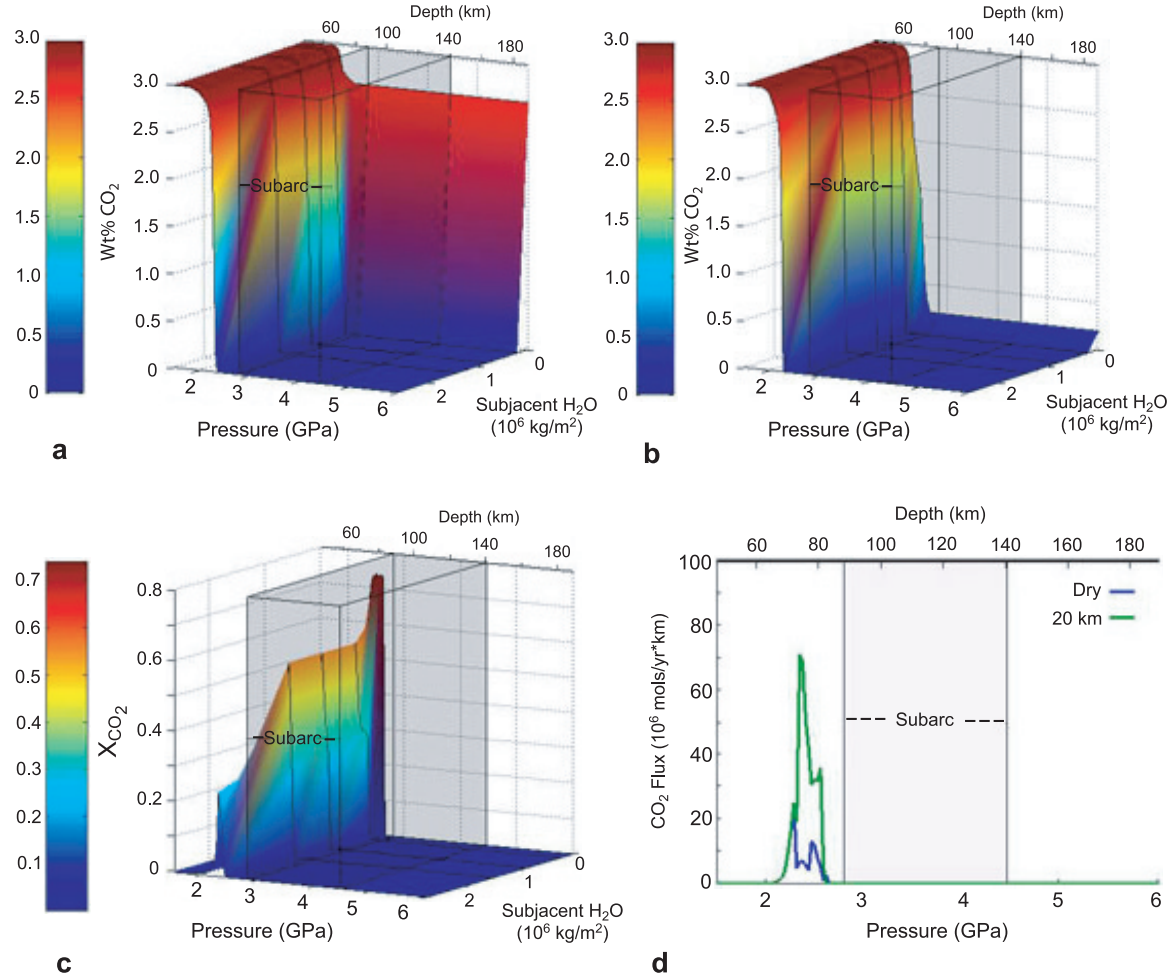


**Figure 5.** Results of infiltration decarbonation models for warm subduction. (a) Decarbonation trend for metabasalt lithology. (b) Decarbonation trend for GLOSS. (c) Composition of fluid evolved from the top of the subducting slab. (d) $CO_2$ flux from the top of the slab. Magnitude of flux is dependent on subjacent lithospheric hydration. For clarity, only two cases are shown: (1) anhydrous lower crust and mantle ("Dry") and (2) mantle hydration extending to 20 km ("20 km").

between a nearly pure $H_2O$ fluid ($X_{CO2}$ ~0.05) to a fluid with $X_{CO2} \sim 0.74$ (Figure 5c). The maximum $CO_2$ content of the fluid is achieved for models with no subjacent $CO_2$, and decreases with increasing degree of lithospheric hydration.

## 4. Discussion

[18] The results presented above suggest that the majority of the $CO_2$ flux from the slab occurs in the fore arc. For both distillation and pervasive infiltration models, we predict no $CO_2$ release at subarc depths under warm subduction settings (Figures 2 and 3). For cool subduction, models involving fluid distillation (simulating perfect flow channelization) result in a fore-arc $CO_2$ flux 6 times the subarc flux (Table 1). In contrast, models simulating pervasive fluid infiltration predict $CO_2$ loss under the fore arc, subarc and beyond. However, the subarc $CO_2$ flux is less than 30% of the fore-arc flux (Table 2).

[19] Upper oceanic mantle dehydration, a possible major source of infiltrating $H_2O$ rich fluid, is insignificant for cooler geotherms because hydroxylated minerals remain stable to pressures beyond the arc. The major $H_2O$ pulse from the mantle is predicted to infiltrate the overlying crust at pressures exceeding 5 GPa. For warmer subduction zones, mantle dehydration is equally ineffective in driving decarbonation at subarc depths because hydrous minerals break down within the fore arc and thus do not provide a subjacent water source for subarc $CO_2$ loss. However, the oceanic upper

mantle can be an important source of $H_2O$-rich fluid for driving decarbonation under thermal conditions intermediate to the extremes considered in the preceding section, as has been demonstrated elsewhere [*Connolly*, 2005]. This possibility is explored further in the following sections.

[20] For our infiltration models, the primary source of $CO_2$ evolved in the subarc is the metabasalt lithology. The marine sediment lithology used in our models of warm and cool subduction (GLOSS) loses nearly all of its original $CO_2$ under the fore arc. The disparity in-depth of decarbonation is largely a function of the original mineral bound water content. Thus it is likely that sediment lithologies containing less $H_2O$ could retain carbonate to depths such as to be a contributor of $CO_2$ to arc volcanism.

### 4.1. Comparison to Modern Subduction Zone Volcanic $CO_2$ Output

[21] Using the same methodology employed to calculate the $CO_2$ fluxes for our base models of cool and warm subduction in the above section, we predict $CO_2$ output for three convergent margins: NE Japan (Honshu), Cascadia, and Central America. This is done to test the veracity of our results and to evaluate the extent to which evolved fluid interacts with rocks in subducting crust. In contrast to our models of cool and warm subduction using average subducting compositions, we utilized bulk compositions for sediment entering subduction zones [*Plank and Langmuir*, 1998] and crustal compositions with age-dependent hydration and carbonation [*Alt and Teagle*, 1999; *Jarrard*, 2003].

[22] In a recent study, *Hilton et al.* [2002] tabulate the $CO_2$ fluxes from 11 volcanic arcs worldwide by utilizing an extensive database of $CO_2/SO_2$ observations and assuming a power law distribution for $SO_2$ flux from arc volcanoes. Using their approach along with volcanic degassing data compiled by *Andres and Kasgnoc* [1998], we estimate that the $CO_2$ flux from the ~1050 km of the Honshu volcanic arc is approximately $45.6 \times 10^9$ mols $CO_2$/yr. In Figure 6, our prediction for the flux of $CO_2$ from the top of the subducting slab along the Honshu P-T path is shown. For distillation decarbonation, the total integrated flux beneath the subarc is ~1.0 Mmols $CO_2$/yr/km arc length (Figure 6a). For the Honshu volcanic arc, the total flux in the subarc amounts to only $1.1 \times 10^9$ mols $CO_2$/yr. In fact, even when combined with the fore-arc $CO_2$ flux, the total $CO_2$ output predicted by our distillation decarbonation models is only ~$9.8 \times 10^9$ mols $CO_2$/yr. For infiltration driven decarbonation, the total integrated flux beneath the subarc is dependent on the extent of subjacent lithospheric hydration and ranges between ~5.0 to 15.7 Mmols/yr/km arc length (Figure 6b). For the ~1050 km of the Honshu volcanic arc, the total subarc flux is $5.3 \times 10^9$–$16.6 \times 10^9$ mols $CO_2$/yr. Our predicted values fall well short of the estimates based on extrapolation from direct volcanic output. One explanation for this shortfall is that the Honshu geotherm is somewhat cooler than assumed in the model presented here. Cooler geothermal conditions have the potential to increase both the efficacy and depth of infiltration-driven decarbonation [*Connolly*, 2005]. An alternative explanation for the predicted shortfall in $CO_2$ subarc output is that the transport of $CO_2$ to arc magma generation in the mantle wedge does not occur by simple vertical flow from the slab but rather as a result of alteration of the fore-arc mantle wedge and subsequent downward drag. Low velocity ($V_P$ and $V_S$) anomalies above the slab below 60 km depth are consistent with alteration of the Honshu fore-arc mantle wedge [*Mishra et al.*, 2003]. The source of mantle wedge serpentinization is generally assumed to be $H_2O$-rich fluids derived from the dehydration of the subducting slab. From Figure 6, it is evident that (1) pulses of $CO_2$ tend to accompany pulses of $H_2O$ and (2) a large pulse of $H_2O$-$CO_2$ fluid is released from the slab in the depth range 60–70 km beneath the fore-arc mantle wedge. For infiltration models, the $34.3 \times 10^9$ mols of $CO_2$/yr released beneath the fore arc, when combined with the subarc flux gives a range of $39.6$–$50.9 \times 10^9$ mols of $CO_2$/yr, which is in good agreement with the measured $CO_2$ flux.

[23] For Cascadia, our results (Figure 7) suggest that for the assumed geothermal conditions no $CO_2$ should be supplied by the subducting slab to the overlying mantle wedge arc magma sources at subarc depths. Under the fore arc, the $CO_2$ flux ranges from $4.2 \times 10^9$ mols $CO_2$/yr for distillation decarbonation (Figure 7a) and up to $10.5 \times 10^9$ mols $CO_2$/yr for infiltration decarbonation (Figure 7b). On the basis of tomographic evidence, *Bostock et al.* [2002] concluded that the fore-arc mantle wedge of the Cascadian arc is likely to be highly serpentinized. Extensive serpentinization of the Cascadian fore-arc mantle wedge supports our prediction that under warm subduction $CO_2$ is driven off the subducting slab under the fore arc by the influx of $H_2O$-rich fluid. In contrast to our results, *James et al.* [1999] predict a flux of $7.7 \times 10^6$ mols $CO_2$/yr per kilometer of the Cascadian volcanic arc. For the

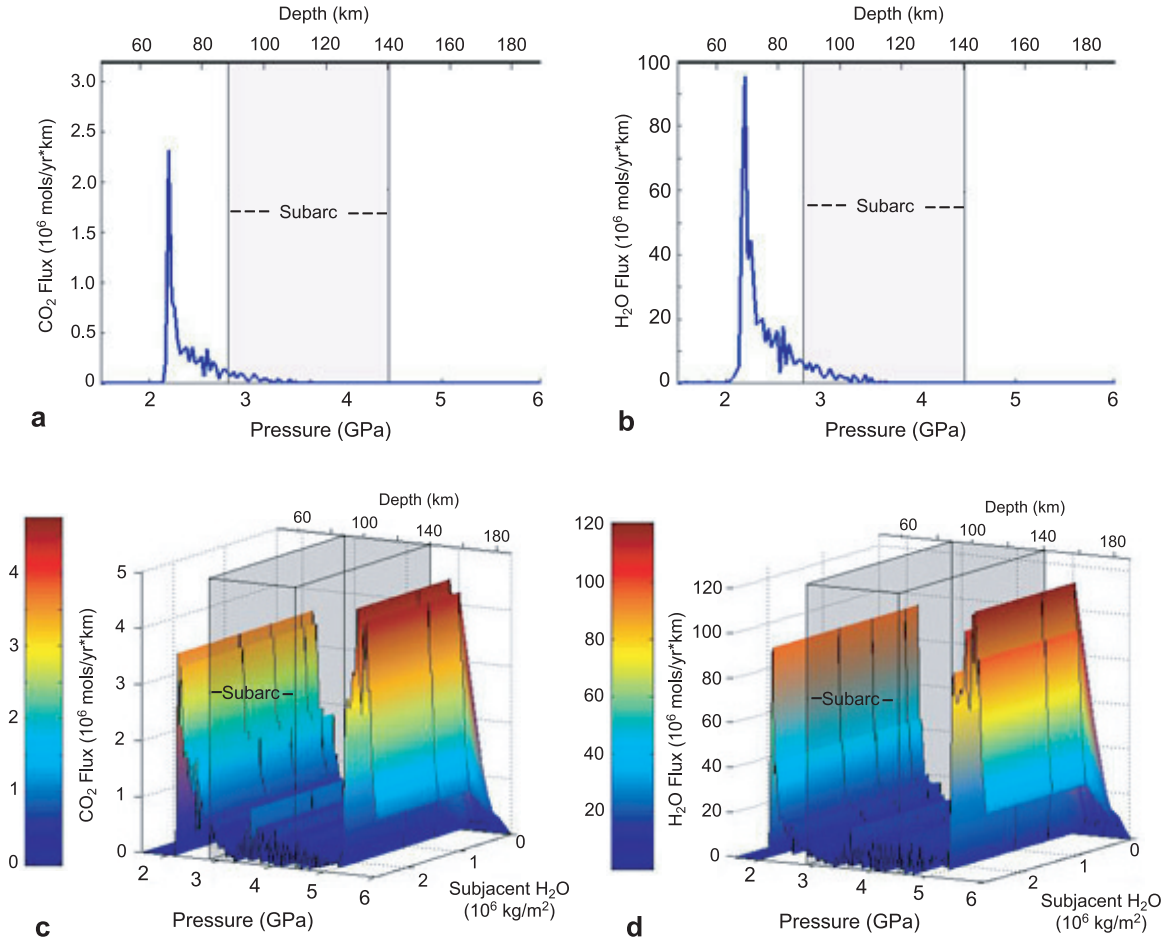


**Figure 6.** $CO_2$ and $H_2O$ fluxes from the top of the subducting slab for Honshu. (a) $CO_2$ flux calculated assuming pure channelization of evolved fluid (distillation). (b) $H_2O$ flux calculated channelized flow. (c) $CO_2$ flux calculated assuming pervasive fluid flow. (d) $H_2O$ flux calculated assuming pervasive fluid flow.

entire 990 km arc length, this flux gives a total output of $7.7 \times 10^9$ mols $CO_2$/yr, an observation that could be explained by cooler geothermal conditions. Nevertheless, our prediction that slab devolatilization occurs primarily in the fore arc is in good agreement with observations of the chemistry of erupted arc lavas [*Rose et al.*, 2001; *Leeman et al.*, 2005; *Green and Sinha*, 2005]. For this scenario, a source for volcanic $CO_2$ in Cascadia would be contamination from the lithosphere below the volcanic arc. *Leeman et al.* [2005] suggest that the relatively weak slab signature of arc lavas in Cascadia may result from melting of lithospheric mantle containing a "stored" slab-derived component from earlier subduction.

## 4.2. Central American Subduction Zone Volcanic Output

[24] The $CO_2$ flux for distillation and infiltration decarbonation in Nicaragua are shown in Figures 8a and 8b, respectively. We use the thermal model for Nicaragua from *Peacock et al.* [2005], which is intermediate between the cooler Honshu model and the warmer Cascadia model. Unlike Honshu and Cascadia, the lithosphere subducting beneath Nicaragua contains a carbonate-rich sedimentary layer [*Plank and Langmuir*, 1998] which provides an additional source of $CO_2$ for arc volcanism. For distillation decarbonation (Figure 8a), the total integrated flux beneath the subarc is ~0.3 Mmols $CO_2$/yr/km arc length. Scaling this figure to the entire ~1500 km of the Central American volcanic arc gives just $0.4 \times 10^9$ mols $CO_2$/yr. For infiltration-driven decarbonation (Figure 8b), the total integrated flux beneath the subarc is dependent on the extent of subjacent lithospheric hydration and ranges between ~2.4 to 43.6 Mmols/yr/km arc length. For the ~1500 km of the Central American volcanic arc, this flux amounts to $3.6 \times 10^9$–$65.6 \times 10^9$ mols $CO_2$/yr. *Hilton et al.* [2002] predict a value of $57.5 \times 10^9$ mols/yr for the

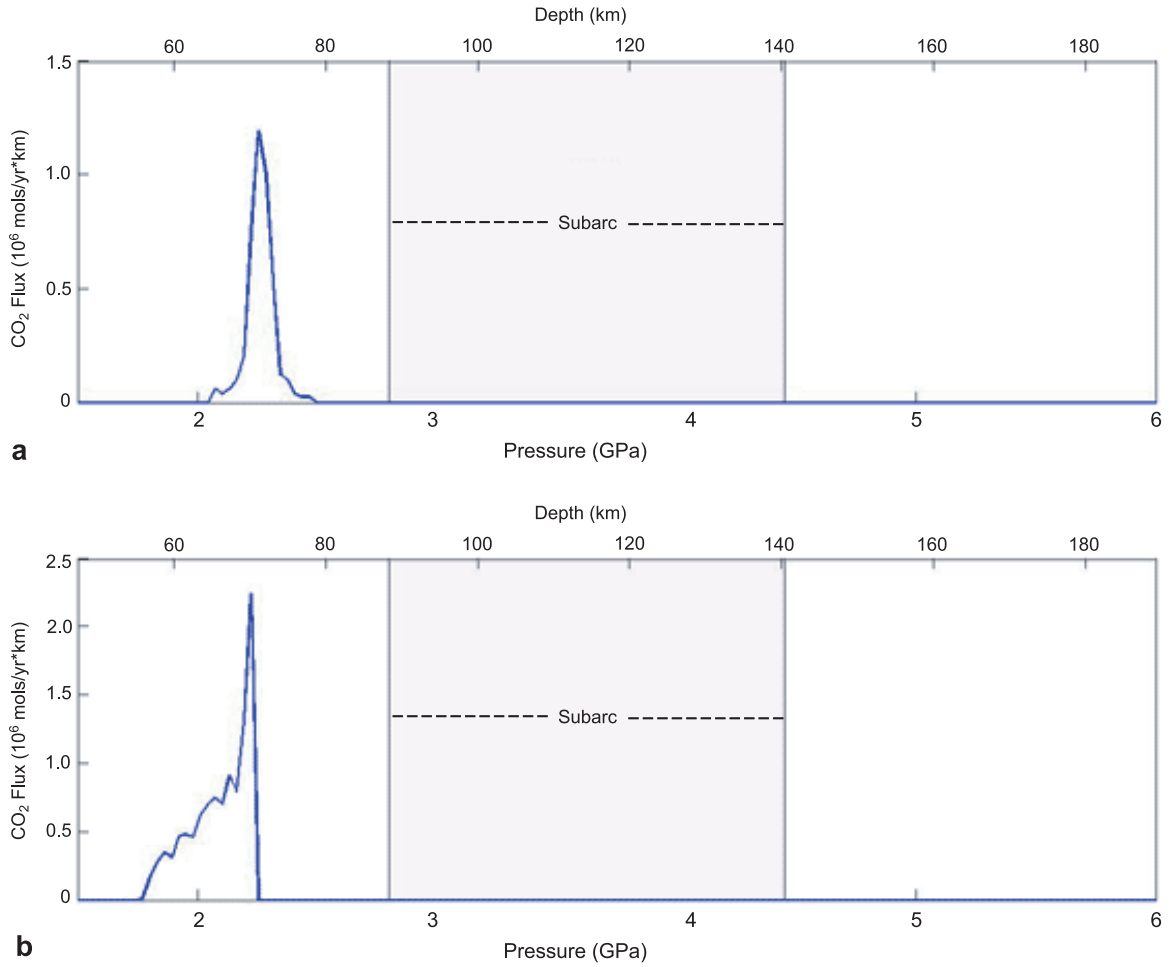


**Figure 7.** $CO_2$ and $H_2O$ fluxes from the top of the subducting slab for Cascadia. (a) $CO_2$ flux calculated assuming pure channelization of evolved fluid (distillation). (b) $CO_2$ flux calculated assuming pervasive fluid flow.

$CO_2$ flux from the Central American arc, which is in agreement with the upper end of our predicted range. Additionally, *Shaw et al.* [2003] predict a $CO_2$ flux of $71 \times 10^9$ mols $CO_2$/yr for the Central American derived from $CO_2/^3He$ relationships, which is also in close agreement with our maximum computed $CO_2$ flux. Further, *Snyder et al.* [2001] predict that $CO_2$ lost from subducted sediments contributes 85–98% of the total $CO_2$ flux from the Central American volcanic arc. This range is in good agreement with our prediction (from fluid infiltration models) that ~84% of the $CO_2$ flux in the subarc is the result of decarbonation of marine sediments (Table 3). As was the case with Honshu and Cascadia, the upper end of our predicted range of decarbonation is for models that include mantle hydration to a depth of 20 km below the base of the oceanic crust. Although *Ranero and Sallarès* [2004] inferred the mantle beneath the subducting Nazca plate may be extensively serpentinized to depths reaching approximately 20 km, hydration of the oceanic upper mantle to such depths is controversial [*Kerrick*, 2002]. Nevertheless, inspection of Table 3 reveals that because the mantle does not dehydrate at subarc depths the total $CO_2$ flux at subarc depths predicted by models involving an extensively hydrated mantle does not differ from models where only the lower crust provides a source of infiltrating $H_2O$. Similar to Honshu, fluid derived from dehydration of the oceanic upper mantle subducting beneath Central America is predicted to infiltrate the upper crust and sediments at depths beyond the subarc. However, other thermomechanical models developed specifically for Nicaragua [*Ruepke et al.*, 2002] do predict mantle dehydration at subarc depth, in which case the extent of hydration of the oceanic mantle is a major factor controlling decarbonation [*Connolly*, 2005].

[25] The upper end of our predicted range of $CO_2$ flux from the Central America arc is for pervasive

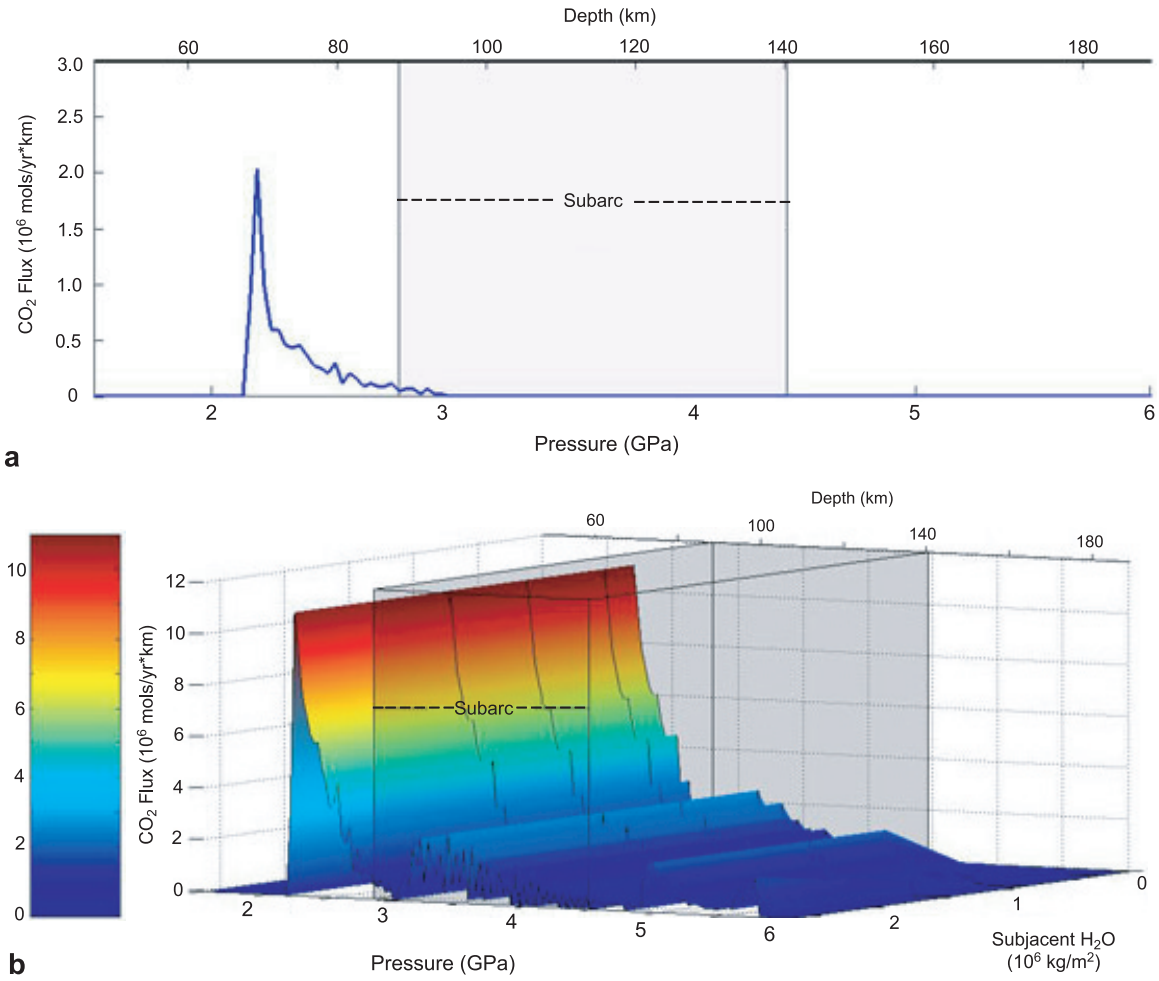


**Figure 8.** $CO_2$ and $H_2O$ fluxes from the top of the subducting slab for Central America. (a) $CO_2$ flux calculated assuming pure channelization of evolved fluid (distillation). (b) $CO_2$ flux calculated assuming pervasive fluid flow.

infiltration models, requiring fluid-rock equilibrium throughout the entire subducting lithospheric section. Because some degree of fluid channelization is likely such that sections of the crust will remain relatively unaltered [*Breeding et al.*, 2003], our flux estimate may overestimate the actual degree of decarbonation. For decarbonation models simulating flow channelization (distillation models), the flux of $CO_2$ beneath the subarc ($0.4 \times 10^9$ mols $CO_2$/yr) falls well short of the observed value, suggesting that distillation decarbonation alone cannot account for the observed $CO_2$ flux. Therefore, although some flow channelization in subducting lithosphere is possible, our results suggest a significant pervasive component to the overall flow regime.

**Table 3.** Sources for $CO_2$ Flux at Subarc Depths for Central America Decarbonation Models

| | $CO_2$ Lost From Sediments, $10^9$mols/yr | $CO_2$ Lost From Oceanic Crust, $10^9$mols/yr | % of Total $CO_2$ Flux From Sediments |
|---|---|---|---|
| Fluid distillation model | 0.0 | 0.4 | 0.0 |
| Fluid infiltration model (anydrous subjacent lithosphere) | 1.4 | 2.2 | 37.6 |
| Fluid infiltration model (lower crustal gabbro hydration only) | 55.4 | 10.2 | 84.4 |
| Fluid infiltration model (20 km upper mantle hydration) | 55.4 | 10.2 | 84.4 |

### 4.3. Global $CO_2$ Flux Estimates

[26] Numerous attempts have been made to quantify the global flux of $CO_2$ from convergent margins and subaerial volcanism in general. These calculations are based on measurements of $CO_2$ and $SO_2$ emission from volcano plumes as well as $CO_2$ degassing from volcano flanks, cold spring $CO_2$ emission, or calculated from magma emplacement rates. These measurements tend to be confined to volcanic arcs, and estimates of total $CO_2$ flux are made assuming the majority of flux occurs above the portion of the slab where arc magmas are generated (i.e., the volcanic arc). One of the common features of the decarbonation and $CO_2$ flux trends observed in this study is that a large proportion of the $CO_2$ lost during subduction occurs at shallow depths beneath the fore arc. Although some of this $CO_2$ will likely be sequestered in ophicarbonates resulting from alteration of the shallow mantle wedge tip, it is also likely that the evolved $CO_2$-bearing fluid will be lost from the system, perhaps via migration up the slab-mantle interface. Indeed, the common observation of low salinity fluids emanating from accretionary wedges stands as evidence for deeply derived fluids reaching the surface [*Moore and Vrolijk*, 1992]. Thus estimations of the $CO_2$ flux from convergent margins based on measurements taken with the associated volcanic arc may grossly underestimate the actual quantity of $CO_2$ evolved from the slab. Additionally, estimates of $CO_2$ degassing based on calculated magma emplacement rates and $CO_2$ content of volcanic products may yield equally erroneous results.

[27] Using the same methodology employed to calculate the $CO_2$ fluxes from Honshu, Cascadia, and Central America, we calculate the $CO_2$ flux for the remaining 38 subduction zones tabulated by *Jarrard* [2003] in order to estimate the global convergent margin $CO_2$ flux. This endeavor is complicated by the lack of sophisticated thermal models for all global subduction zones. Nevertheless, we provisionally assume that the thermal profiles of subduction zones intermediate between the Honshu and Cascadia end-members can be linearly scaled by age of incoming plate and convergence rate. Using these derivative thermal models with the marine sediment data of *Plank and Langmuir* [1998] and estimates of crustal hydration and carbonation [*Staudigel et al.*, 1989; *Alt and Teagle*, 1999; *Carlson*, 2003; *Carlson and Miller*, 2004], we calculate total $CO_2$ flux from subduction zones. For subduction zones where bulk composition data for incoming sediment was not available, we used the global average subducting sediment composition (GLOSS) from *Plank and Langmuir* [1998].

[28] For the 41 subduction zones outlined by *Jarrard* [2003], our calculated $CO_2$ fluxes are given in Table 4. For each trench, we show fluxes based on pure channelization (distillation) and two models assuming pervasive infiltration: one where sources of infiltrating fluid are confined to the crust and another assuming a 20 km thick section of hydrated upper mantle. From the data in Table 4, the calculated range for $CO_2$ flux at subarc depths is $0.03 \times 10^{12}$–$0.94 \times 10^{12}$ mols/yr, which is in good agreement with estimates by *Snyder et al.* [2001] based on volatile measurements from the Central American arc ($0.04 \times 10^{12}$–$0.37 \times 10^{12}$ mols $CO_2$/yr). However, the bulk of the $CO_2$ flux from convergent margins is predicted to occur at fore-arc depths. From Table 4, the total (fore arc + subarc) global $CO_2$ flux from convergent margins is $0.35 \times 10^{12}$–$3.12 \times 10^{12}$ mols/yr. This range is in good agreement with several previous estimates of arc volcanic flux ($0.04 \times 10^{12}$–$0.37 \times 10^{12}$ mol/yr [*Snyder et al.*, 2001]; $2.5 \times 10^{12}$ mol/yr [*Marty and Tolstikhin*, 1998]; $3.1 \times 10^{12}$ mol/yr [*Sano and Williams*, 1996]). The agreement between these estimates and our combined fore-arc and subarc $CO_2$ fluxes may imply that downdrag of altered fore-arc mantle wedge could be an important mechanism for providing $CO_2$ for arc volcanism. However, as discussed in the following section of the paper, there are other explanations for this agreement. Regardless, $CO_2$ evolved in the fore arc that is not entrained in mantle wedge downdrag, although not contributing to arc *volcanism*, is still an important part of the overall arc $CO_2$ budget.

[29] The data in Table 4 suggest that for the majority of subduction zones, dehydration of serpentinized oceanic upper mantle does not provide a fertile $H_2O$ source for driving decarbonation at fore-arc or subarc depths. For most cool and intermediate subduction zones, fluid derived from dehydration of the oceanic upper mantle is predicted to infiltrate the upper crust and sediments at depths beyond the subarc. The only two subduction zones where upper mantle water sources are relevant to decarbonation are the Aegean and Mexico trenches. For all subduction zones warmer than Mexico, dehydration of the lower crust alone is sufficient to drive off any carbonate within the crust and marine sedi-

**Table 4.** Flux for All 41 Subduction Zones Tabulated by *Jarrard* [2003][a]

| | Distillation | | | Infiltration, Crustal Hydration Only | | | Infiltration, 20 km Upper Mantle Hydration | | | |
|---|---|---|---|---|---|---|---|---|---|---|
| Subduction Zone | Fore Arc, $10^9$ mols $CO_2$/yr | Subarc, $10^9$ mols $CO_2$/yr | Total, $10^9$ mols $CO_2$/yr | Fore Arc, $10^9$ mols $CO_2$/yr | Subarc, $10^9$ mols $CO_2$/yr | Total, $10^9$ mols $CO_2$/yr | Fore Arc, $10^9$ mols $CO_2$/yr | Subarc, $10^9$ mols $CO_2$/yr | Total, $10^9$ mols $CO_2$/yr | $CO_2$ Retained Beyond Subarc, % original $CO_2$ |
| Honshu | 8.6 | 1.1 | 9.8 | 34.3 | 16.6 | 50.9 | 34.3 | 16.6 | 50.9 | 68.5 |
| Tonga | 26.5 | 2.3 | 28.8 | 134.2 | 62.2 | 196.4 | 134.2 | 62.2 | 196.4 | 47.0 |
| E. Sunda | 9.8 | 1.2 | 10.9 | 83.2 | 35.9 | 119.1 | 83.2 | 35.9 | 119.1 | 59.9 |
| Kurile | 10.7 | 1.2 | 11.9 | 45.1 | 20.5 | 65.6 | 45.1 | 20.5 | 65.6 | 59.5 |
| Kamchatka | 7.1 | 1.0 | 8.1 | 35.4 | 14.4 | 49.8 | 35.4 | 14.4 | 49.8 | 55.1 |
| Izu-Bonin | 5.9 | 1.0 | 6.9 | 52.8 | 19.5 | 72.3 | 52.8 | 19.5 | 72.3 | 66.8 |
| Java | 13.2 | 1.1 | 14.3 | 72.6 | 32.7 | 105.3 | 72.6 | 32.7 | 105.3 | 38.7 |
| Mariana | 9.2 | 1.5 | 10.7 | 74.7 | 34.8 | 109.5 | 74.7 | 34.8 | 109.5 | 56.7 |
| New Britain[b] | 8.1 | 1.5 | 9.6 | 79.2 | 32.0 | 111.2 | 79.2 | 32.0 | 111.2 | 41.3 |
| Kermadec | 9.0 | 0.8 | 9.8 | 51.5 | 35.1 | 86.6 | 51.5 | 35.1 | 86.6 | 27.6 |
| Vanuatu | 21.5 | 2.3 | 23.8 | 211.9 | 86.2 | 298.1 | 211.9 | 86.2 | 298.1 | 35.4 |
| Makran | 5.4 | 0.3 | 5.7 | 84.2 | 23.9 | 108.1 | 84.2 | 23.9 | 108.1 | 82.4 |
| E. Aleutian | 8.5 | 0.8 | 9.2 | 49.0 | 32.4 | 81.4 | 49.0 | 32.4 | 81.4 | 26.1 |
| Sumatra | 18.7 | 3.7 | 22.4 | 39.1 | 32.2 | 71.3 | 39.1 | 32.2 | 71.3 | 62.5 |
| N. Chile[b] | 15.5 | 1.0 | 16.5 | 116.9 | 50.1 | 167.0 | 116.9 | 50.1 | 167.0 | 45.7 |
| Phillipine | 13.0 | 0.7 | 13.7 | 110.7 | 47.5 | 158.2 | 110.7 | 47.5 | 158.2 | 14.2 |
| Alaska | 7.5 | 1.5 | 9.0 | 31.7 | 29.1 | 60.8 | 31.7 | 29.1 | 60.8 | 51.3 |
| Ryukyu | 8.3 | 0.5 | 8.8 | 44.5 | 27.6 | 72.1 | 44.5 | 27.6 | 72.1 | 14.1 |
| Scotia | 5.6 | 0.3 | 5.9 | 30.8 | 24.4 | 55.2 | 30.8 | 24.4 | 55.2 | 10.7 |
| San Cristobal[b] | 6.9 | 0.5 | 7.4 | 56.5 | 24.3 | 80.8 | 56.5 | 24.3 | 80.8 | 15.0 |
| Peru | 14.5 | 0.7 | 15.2 | 113.4 | 42.9 | 156.3 | 113.4 | 42.9 | 156.3 | 40.7 |
| Hikurangi[b] | 0.8 | 0.7 | 1.5 | 1.6 | 3.6 | 5.2 | 1.6 | 3.6 | 5.2 | 86.9 |
| N. Antilles | 1.7 | 0.1 | 1.8 | 8.6 | 5.4 | 14.0 | 8.6 | 5.4 | 14.0 | 11.0 |
| S. Antilles | 1.4 | 0.3 | 1.7 | 2.4 | 2.6 | 5.0 | 2.4 | 2.6 | 5.0 | 84.0 |
| Andaman | 2.6 | 1.1 | 3.8 | 3.0 | 2.4 | 5.4 | 3.0 | 2.4 | 5.4 | 94.0 |
| C. Chile[b] | 9.8 | 2.4 | 12.1 | 125.0 | 52.8 | 177.8 | 125.0 | 52.8 | 177.8 | 85.7 |
| Columbia | 11.2 | 0.4 | 11.6 | 82.9 | 12.3 | 95.2 | 82.9 | 12.3 | 95.2 | 81.4 |
| W. Aleutian[b] | 2.4 | 0.1 | 2.6 | 13.4 | 12.0 | 25.4 | 13.4 | 12.0 | 25.4 | 15.3 |
| N. Sulawesi[b] | 2.6 | 0.3 | 2.9 | 28.1 | 11.6 | 39.7 | 28.1 | 11.6 | 39.7 | 14.8 |
| C. America | 13.3 | 0.4 | 13.7 | 138.3 | 65.6 | 203.9 | 138.3 | 65.6 | 203.9 | 78.4 |
| Trobriand[b] | 1.8 | 0.4 | 2.1 | 21.2 | 9.2 | 30.4 | 21.2 | 9.2 | 30.4 | 44.8 |
| Nankai | 4.1 | 0.0 | 4.2 | 25.1 | 3.9 | 29.0 | 25.1 | 3.9 | 29.0 | 5.1 |
| Cotabato[b] | 1.7 | 0.0 | 1.7 | 14.4 | 4.1 | 18.5 | 14.4 | 4.1 | 18.5 | 2.5 |
| Aegean[b] | 0.8 | 0.3 | 1.1 | 12.4 | 7.0 | 19.4 | 12.4 | 23.3 | 35.7 | 0.0 |
| Mexico | 11.4 | 0.0 | 11.4 | 32.9 | 3.5 | 36.4 | 32.9 | 4.0 | 36.9 | 0.0 |
| Negros[b] | 1.7 | 0.0 | 1.7 | 14.6 | 0.4 | 15.0 | 14.6 | 0.4 | 15.0 | 0.0 |
| Sulu[b] | 2.1 | 0.0 | 2.1 | 14.0 | 0.5 | 14.5 | 14.0 | 0.5 | 14.5 | 0.0 |
| Manila[b] | 1.9 | 0.0 | 1.9 | 10.7 | 0.5 | 11.2 | 10.7 | 0.5 | 11.2 | 0.0 |
| S. Chile[b] | 6.7 | 0.0 | 6.7 | 69.9 | 1.0 | 70.9 | 69.9 | 1.0 | 70.9 | 0.0 |
| Yap-Palau[b] | 1.3 | 0.0 | 1.3 | 2.4 | 0.0 | 2.4 | 2.4 | 0.0 | 2.4 | 0.0 |
| Cascadia | 4.2 | 0.0 | 4.2 | 10.8 | 0.0 | 10.8 | 10.8 | 0.0 | 10.8 | 0.0 |
| **Total (Global)** | 317.1 | 31.4 | **348.5** | 2183.4 | 922.7 | **3106.1** | 2183.4 | 939.5 | **3122.9** | |

[a] Subduction zones are listed in order of increasing approximate relative warmth (see text for details).
[b] Trenches where GLOSS [*Plank and Langmuir*, 1998] was used to approximate the composition of the incoming sediment column.

mentary units. Thus our liberal model assumptions regarding the hydration of the oceanic mantle have not inflated our estimation of global $CO_2$ flux from convergent margins. Consequently, on the basis of our observation that $CO_2$ flux predicted from pervasive infiltration models more closely coincides with observed $CO_2$ output from individual arcs, the higher end of our predicted global $CO_2$ flux range ($\sim 3.1 \times 10^{12}$ mol/yr) is favored. Assuming that mid-ocean ridges do not provide a net source of $CO_2$ degassing [*Kerrick*, 2001], our estimates for $CO_2$ flux from convergent margins suggest significant $CO_2$ emission from other geologic regimes would be required to balance drawdown of atmospheric $CO_2$ by the weathering of

silicates [*Varekamp and Thomas*, 1998; *Berner and Kothavala*, 2001; *Berner*, 2004].

## 4.4. Subduction Zone $CO_2$ Recycling

[30] Despite the enhanced effect of infiltration on decarbonation, our study implies that a significant proportion of original carbonate is retained within the slab beyond the subarc. For fluid infiltration models incorporating 20 km of hydrated mantle, Table 4 gives the percentage of original carbonate that is retained beyond the volcanic arc for the 41 subduction zones examined in the previous section. For the warmest subduction zones, complete $CO_2$ loss is predicted. However, for cool and intermediate subduction, up to ~80% of original carbonate is retained within the slab. Although the extent of hydration of the oceanic upper mantle remains contentious, the upper mantle serpentinization considered in this study is representative of what is believed to be maximum hydration conditions [*Connolly*, 2005]. Additionally, our infiltration analysis assumes pervasive fluid flow and thus maximizes fluid-rock interaction. However, the decarbonation effect of infiltrating fluid may be lessened within the subducting lithosphere due to channelized flow [*Breeding et al.*, 2003]. Taken together with these observations, our results support the hypothesis that a considerable proportion of carbonate is retained within the slab and is subducted into the deeper mantle. Furthermore, our study underscores a strong correlation between extensive subduction zone decarbonation and warm subduction settings. Although Honshu and Cascadia are representative of the range of thermal conditions in modern arcs, the temperature of the Archean mantle may have been as much as 200°C warmer than today [*Abbott et al.*, 1994; *Komiya*, 2001], thereby resulting in warmer subduction thermal regimes. Our prediction that subducting slabs experience complete decarbonation under warm subduction settings is therefore consistent with the observation that mantle-derived, carbonate rich melts (e.g., carbonatites) are virtually absent from the Archean record and increase in frequency throughout the Proterozoic and Phanerozoic [*Wooley*, 1989], coincident with a general cooling of the Earth over this time period.

## 4.5. Uncertainties/Caveats

[31] Accurate modeling of decarbonation of subducting lithologies is dependent upon numerous parameters, many of which are subject to considerable uncertainty. As noted previously, slab devolatilization depends strongly upon the assumed thermal regime. The ability to accurately represent the subduction thermal regime, however, is limited by uncertainty regarding the depth and nature of slab/mantle wedge coupling, properties of the wedge tip, and rheology of the mantle wedge [*van Keken et al.*, 2002]. Although robust thermal models which account for temperature and stress dependent rheology of the mantle wedge are available for Honshu and Cascadia [*van Keken et al.*, 2002] as well as Central America [*Peacock et al.*, 2005], the thermal state of most global subduction zones is loosely constrained. As more thermal models for the convergent margins become available, our ability to quantity decarbonation of subducting slabs will improve.

[32] Our prediction that $CO_2$ release from the slab occurs mainly in the fore arc for most subduction zones is dependent on our assumed fore-arc and subarc depth ranges. For some arcs (i.e., those with depths to slab of 80–90 km), our predicted $CO_2$ release may be coincident with subarc depths. However, for most arcs (those with depths to slab of 100–120 km), we predict subduction zone decarbonation occurs predominantly at fore-arc depths.

[33] As previously discussed, our predictions of subduction zone metamorphic decarbonation are critically dependent on the mobility and propagation mechanism of slab-derived fluids. Although the mobility of slab-derived fluids under high pressure conditions remains uncertain [e.g., *Scambelluri and Philippot*, 2001], recent work by *John et al.* [2004] supports the mechanism of fluid infiltration for driving prograde metamorphism in subducting lithologies. However, the efficiency of infiltration-induced decarbonation will be limited by the extent of the fracture network within lithosphere entering subduction zones and the degree to which this network remains open with increasing pressure, both of which remain poorly constrained. Additionally, we have assumed fluids evolved from devolatilization are transported upward immediately and have not implemented mechanical constraints on fluid propagation. *Scambelluri and Philippot's* [2001] contention is supported by mechanical models that suggest metamorphic fluid expulsion may be episodic [*Connolly*, 1997] in which case a batch fractionation model may be appropriate to understanding the dynamics of slab devolatilization. Coupling of mass transport models with our models of open system decarbonation is

beyond the scope of our current analysis and warrants further research.

[34] Although the composition of sedimentary units entering subduction zones is constrained by ODP data [*Plank and Langmuir*, 1998; *Plank et al.*, 2000], tectonic imbrication and underplating will result in a different profile of lithologies than those predicted by observations of sediment columns approaching trenches, thereby complicating the comparison of our results with active subduction systems. These uncertainties are mitigated by our approach of using *Plank and Langmuir*'s [1998] bulk composition of sedimentary columns entering subduction zones, which represent average sediment composition for each subduction zone as opposed to actual lithologic units. Although using average sediment composition for each subduction zone instead of actual lithologic units does affect our results for global $CO_2$ arc flux, computation of devolatilization for each individual lithology entering subduction zones is beyond the scope of this preliminary analysis of open system behavior. Additionally, sources of $CO_2$ not considered in this study such as material scraped off the overriding plate by tectonic erosion [*Vannucchi et al.*, 2003] and subduction of organic carbon [*Bebout*, 1995] await future analysis.

[35] The amount of $CO_2$ released from carbonate-bearing lithologies is a function of bulk composition and hence mineralogy. Thus, for example, during subduction metamorphism pure carbonate oozes would not undergo decarbonation. The common occurrence of marbles in ultrahigh-pressure (UHP) metamorphic terranes [*Compagnoni and Rolfo*, 1999] attest to the incomplete decarbonation of deeply subducted carbonate-rich sediments. In contrast, marls would provide a fertile $CO_2$ source lithology. Such lithologic variations should be considered in further research on subduction zone metamorphic decarbonation of marine sediment lithologies.

[36] Compared to marine sediments and upper crustal extrusives, the composition of the lower crust is much more poorly defined. The minimal extent of hydration and carbonation of the lower crust as assumed in this study is based on the limited database of ODP cores that have been recovered from the lower crustal extrusives and gabbroic units. If future drilling of the oceanic crust reveals more extensive alteration than has been assumed here, our results will need to be modified accordingly. Still less is known about the in situ composition of the oceanic upper mantle. Although this layer is exposed in ophiolites worldwide, ophiolites may not be representative of in situ oceanic mantle lithologies [*Jarrard*, 2003]. Of particular significance to this study is the ambiguity regarding the volatile budget of the upper mantle. Some authors have argued that outer-rise faulting may provide pathways for seawater penetration and consequent mantle serpentinization [*Peacock*, 2001; *Ranero et al.*, 2003; *Hacker et al.*, 2003; *Ranero and Sallarès*, 2004]; however, this hypothesis remains contentious [*Kerrick*, 2002]. Nevertheless, on the basis of their analysis of relic subducted oceanic crust in central Zambia, *John et al.* [2004] have inferred that eclogitization of crustal gabbros was driven by infiltration of fluids derived from the underlying upper mantle. Although this provides support for a hydrated upper mantle, the extent of serpentinization remains uncertain. Equally uncertain is the $CO_2$ content of the upper mantle. The lithospheric mantle is volumetrically the most significant lithology entering subduction zones, and thus even a small carbonate content could significantly impact the $CO_2$ budgets of convergent margins. However, *Kerrick and Connolly* [1998] have demonstrated that subducted ophicarbonates may remain stable well beyond the subarc.

[37] Although dissolution of carbonate into aqueous fluids remains a potential mechanism for removal of $CO_2$ from subducted lithologies, this mechanism is not likely to be significant along cool subduction paths due to limited dehydration of the crust and upper mantle. For warmer subduction the efficacy of carbonate dissolution is clouded by the fact that the fluid infiltrating carbonate-bearing lithologies may contain up to 20–75 mol% $CO_2$. As a result, the activity of water in the infiltrating fluid will be lowered, thereby reducing $CO_2$ solubility.

[38] Melting of metabasalts represents another alternative mechanism for the transport of $CO_2$ from the slab. Along cool subduction paths, significant metabasalt melting is unlikely to occur even under $H_2O$-saturated conditions [*van Keken et al.*, 2002]. P-T conditions along warmer subduction paths may be favorable for $H_2O$-saturated metabasalt melting; however, the predicted shallow dehydration of the slab makes hydrous melting (and therefore the efficacy of carbonate transport by this mechanism) uncertain. For the case of anhydrous carbonated eclogite, high pressure melting experiments indicate that carbonate remains as a refractory phase in even the hottest subduction

thermal regimes [*Dasgupta et al.*, 2004]. The lack of high pressure melting experiments on carbonate-bearing marine sediments makes evaluation of the efficacy of $CO_2$ transfer due to melting of subducted sediments problematic.

## 5. Conclusions

[39] In this study we have quantified the effects of fluid infiltration and fractionation on decarbonation reactions in subducting lithologies and have evaluated the nature of fluid-rock interaction in the subducting lithosphere. Our distillation (pure fluid channelization) models predict that the quantity of slab-derived $CO_2$ greatly underestimates actual $CO_2$ flux measured from volcanic arcs. In comparison, models assuming pervasive infiltration much more closely predict measured arc $CO_2$ output. As such, it is likely that fluid flow in subducting lithosphere involves a significant pervasive component. Furthermore, our analysis predicts significant $CO_2$ loss at fore-arc depths for the entire range of thermal conditions realized in modern subduction zones. Fore-arc mantle wedge serpentinization (generally assumed to be caused by $H_2O$-rich fluid derived from the subducting slab) is commonly observed in cool (e.g., Honshu [*Mishra et al.*, 2003]), intermediate (e.g., Central America [*DeShon and Schwartz*, 2004]), and warm (e.g., Cascadia [*Bostock et al.*, 2002]) subduction zones. Our $H_2O$ infiltration analysis reveals that pulses of $CO_2$ from the slab to tend to accompany pulses of $H_2O$ (e.g., Figure 6). Thus the large flux of $CO_2$ at fore-arc depths is consistent with the widespread occurrence of fore-arc mantle wedge serpentinization.

[40] For intermediate and warm subduction zones, $CO_2$ flux estimates based on measurements within the volcanic arc alone may significantly underestimate the total flux, given the large proportion of $CO_2$ that is predicted to be lost at fore-arc depths. Globally, we predict that the $CO_2$ flux from convergent margins (fore arc + subarc) is $0.35 \times 10^{12}$–$3.12 \times 10^{12}$ mols $CO_2$/yr, with the lower end of this range derived from our distillation models and the upper end from pervasive infiltration models assuming well hydrated subjacent lithosphere. Given our earlier conclusions regarding the likelihood of pervasive flow in subducting lithosphere, we favor the upper end of this range. Our predicted global $CO_2$ flux from convergent margins is in good agreement with previous estimates of arc volcanic flux ($0.04 \times 10^{12}$–$0.37 \times 10^{12}$ mol/yr [*Snyder et al.*, 2001]; $2.5 \times 10^{12}$ mol/yr [*Marty and Tolstikhin*, 1998]; $3.1 \times 10^{12}$ mol/yr [*Sano and Williams*, 1996]). The agreement between these estimates and our combined fore-arc and subarc $CO_2$ fluxes suggests downdrag of altered fore-arc mantle wedge may be an important mechanism for providing $CO_2$ for arc volcanism. However, an appeal to downdrag to explain subarc volatile fluxes is complicated by two issues: the short timescale for slab-to-arc volatile transport that appears to be necessary to preserve $Be^{10}$ [e.g., *McHargue and Damon*, 1991], and the complex mechanism required to transport volatiles to the subarc region of the mantle wedge [*Davies and Stevenson*, 1992]. In view of these factors, two alternate scenarios to downdrag warrant consideration: (1) infiltration-driven decarbonation is not the dominant mechanism, but rather a batch decarbonation process is operative, in which case it can be argued that a closed system model is an appropriate proxy for the natural process [*Kerrick and Connolly*, 1998, 2001a, 2001b; *Connolly*, 2005], or (2) subduction zone thermal conditions are restricted to a narrower range than considered here, in which case the locus of devolatilization would be shifted to depths more characteristic of the subarc slab [*Connolly*, 2005].

[41] Our estimate of the global $CO_2$ flux generated by subduction zone devolatilization is consistent with that of *Connolly* [2005], but there are significant differences in the details of the devolatilization process depicted by the two studies. In the present study, dehydration of the oceanic mantle has little influence on decarbonation because the dehydration either does not occur within-depth range considered or it occurs beneath the fore arc at conditions where the $CO_2$ solubility is low. In contrast *Connolly* [2005] chose intermediate geothermal conditions, with the result that dehydration of the mantle at subarc depth was the primary cause of infiltration-driven decarbonation. This discrepancy highlights the sensitivity of the models to the assumed geothermal structure. That the two studies yield similar flux estimates reflects the fact that the present study accounts for the sedimentary carbonate budget, whereas that of *Connolly* [2005] does not.

[42] Our results, in accord with those of *Connolly* [2005], suggest that in cool and intermediate subduction thermal regimes carbonate survives beyond the volcanic subarc and is subducted into the deep mantle. Our predicted range of $CO_2$ output from convergent margins ($0.35 \times 10^{12}$–$3.12 \times 10^{12}$ mols $CO_2$/yr) is insufficient to offset drawdown of atmospheric $CO_2$ by silicate weath-

ering [*Varekamp and Thomas*, 1998; *Berner and Kothavala*, 2001; *Berner*, 2004], and thus additional $CO_2$ emission from other geologic regimes (e.g., hot spots) is required to balance the global carbon cycle.

[43] As demonstrated here and elsewhere [*Kerrick and Connolly*, 1998, 2001a, 2001b; *Connolly*, 2005], decarbonation of subducted lithologies is critically dependent on the thermal regime. Rapid subduction leads to cool slabs which undergo limited decarbonation, whereas slow subduction results in warm slabs and significant $CO_2$ production. This observation contradicts the assumption that subduction rate is proportional to $CO_2$ paleoflux from volcanic arcs [*Berner and Kothavala*, 2001]. Accordingly, models which predict the contribution of arc volcanism to paleoatmospheric $CO_2$ levels simply on the basis of seafloor spreading rates [*Berner and Kothavala*, 2001] require reevaluation.

## Acknowledgments

[44] This study represents P. J. Gorman's M.S. thesis research at Penn State. He gratefully acknowledges an NSF Graduate Research Fellowship. We thank Peter van Keken and Simon Peacock for providing subduction zone thermal modeling data. Additionally, we thank Gray Bebout and Jane Selverstone for helpful reviews. This research was supported by National Science Foundation grant OCE 03-05137 (Margins Program) and by a generous grant from Ilka Williams of the IRKA Foundation and by Swiss National Science Foundation grant 200020-101965.

## References

Abbott, D. L., L. Burgess, J. Longhi, and W. H. F. Smith (1994), An empirical thermal history of the Earth's upper mantle, *J. Geophys. Res.*, *99*, 13,835–13,850.

Ague, J. J. (2003), Fluid flow in the deep crust, in *Treatise on Geochemistry*, vol. 3, *Geochemistry of the Crust*, edited by R. Rudnick, pp. 195–228, Elsevier, New York.

Alt, J. C., and D. A. H. Teagle (1999), The uptake of carbon during alteration of ocean crust, *Geochim. Cosmochim. Acta*, *63*, 1527–1535.

Andres, R. J., and A. D. Kasgnoc (1998), A time-averaged inventory of subaerial volcanic sulfur emissions, *J. Geophys. Res.*, *103*, 25,251–25,261.

Bebout, G. E. (1995), The impact of subduction-zone metamorphism on mantle-ocean chemical cycling, *Chem. Geol.*, *126*, 191–218.

Becker, H., K. P. Jochum, and R. W. Carlson (2000), Trace element fractionation during dehydration of eclogites from high-pressure terranes and the implications for element fluxes in subduction zones, *Chem. Geol.*, *163*, 65–99.

Behn, M. D., and P. B. Kelemen (2003), Relationship between seismic P-wave velocity and the composition of anhydrous igneous and meta-igneous rocks, *Geochem. Geophys. Geosyst.*, *4*(5), 1041, doi:10.1029/2002GC000393.

Berner, R. A. (2004), *The Phanerozoic Carbon Cycle: $CO_2$ and $O_2$*, Oxford Univ. Press, New York.

Berner, R. A., and Z. Kothavala (2001), GEOCARB III: A revised model of atmospheric $CO_2$ over Phanerozoic time, *Am. J. Sci.*, *301*, 182–204.

Bostock, M. G., R. D. Hyndman, S. Rondenay, and S. M. Peacock (2002), An inverted continental Moho and serpentinization of the forearc mantle, *Nature*, *417*, 536–538.

Breeding, C. M., J. J. Ague, M. Bröcker, and E. W. Bolton (2003), Blueschist preservation in a retrograded, high-pressure, low-temperature metamorphic terrane, Tinos, Greece: Implications for fluid flow paths in subduction zones, *Geochem. Geophys. Geosyst.*, *4*(1), 9002, doi:10.1029/2002GC000380.

Carlson, R. L. (2003), Bound water content of the lower oceanic crust estimated from modal analyses and seismic velocities of oceanic diabase and gabbro, *Geophys. Res. Lett.*, *30*(22), 2142, doi:10.1029/2003GL018213.

Carlson, R. L., and D. J. Miller (2003), Mantle wedge water contents estimated from seismic velocities in partially serpentinized peridotites, *Geophys. Res. Lett.*, *30*(5), 1250, doi:10.1029/2002GL016600.

Carlson, R. L., and D. J. Miller (2004), Influence of pressure and mineralogy on seismic velocities in oceanic gabbros: Implications for the composition and state of the lower oceanic crust, *J. Geophys. Res.*, *109*, B09205, doi:10.1029/2003JB002699.

Compagnoni, R., and F. Rolfo (1999), Characteristics of UHP pelites, gneisses, and other unusual rocks, *Int. Geol. Rev.*, *41*, 552–570.

Connolly, J. A. D. (1990), Multivariable phase diagrams: An algorithm based on generalized thermodynamics, *Am. J. Sci.*, *290*, 666–718.

Connolly, J. A. D. (1997), Devolatilization-generated fluid pressure and deformation-propagated fluid-flow during prograde regional metamorphism, *J. Geophys. Res.*, *102*, 18,149–18,173.

Connolly, J. A. D. (2005), Computation of phase equilibria by linear programming: A tool for geodynamic modeling and its application to subduction zone decarbonation, *Earth Planet. Sci. Lett.*, *236*, 524–541.

Dasgupta, R., M. M. Hirschmann, and A. C. Withers (2004), Deep global cycling of carbon constrained by the solidus of anhydrous, carbonated eclogite under upper mantle conditions, *Earth Planet. Sci. Lett.*, *227*, 73–85.

Davies, J. H., and D. J. Stevenson (1992), Physical model of source region of subduction zone volcanics, *J. Geophys. Res.*, *97*, 2037–2070.

DeShon, H. R., and S. Y. Schwartz (2004), Evidence for serpentinization of the forearc mantle wedge along the Nicoya Peninsula, Costa Rica, *Geophys. Res. Lett.*, *31*, L21611, doi:10.1029/2004GL021179.

Elliott, T. (2004), Tracers of the slab, in *Inside the Subduction Factory*, *Geophys. Monogr. Ser.*, vol. 138, edited by J. Eiler, pp. 23–45, AGU, Washington, D. C.

Ferry, J. M. (1991), Dehydration and decarbonation reactions as a record for fluid infiltration, *Rev. Mineral.*, vol. 26, edited by D. M. Kerrick, pp. 351–393, Mineral. Soc. of Am., Washington, D. C.

Franz, L., R. L. Romer, R. Klemd, R. Schmid, R. Oberhansli, T. Wagner, and D. Shuwen (2001), Eclogite-facies quartz veins within metabasites of the Dabie Shan (eastern China): Pressure-temperature-time-deformation-path, composition of the fluid phase and fluid flow during exhumation of high-pressure rocks, *Contrib. Mineral. Petrol.*, *141*, 322–346.

Green, N. L., and A. K. Sinha (2005), Consequences of varied slab age and thermal structure on enrichment processes and melting regimes in the sub-arc mantle of the northern Cascadia subduction system, *J. Volcanol. Geotherm. Res.*, *140*, 107–132, doi:10.1016/j.jvolgeores.2004.07.017.

Grove, T. L., S. W. Parman, S. A. Bowring, R. C. Price, and M. B. Baker (2002), The role of an $H_2O$-rich fluid component in the generation of primitive basaltic andesites and andesites from the Mt. Shasta region, N. California, *Contrib. Mineral. Petrol.*, *142*, 375–396.

Hacker, B. R., S. M. Peacock, G. A. Abers, and S. D. Holloway (2003), Subduction factory 2. Are intermediate-depth earthquakes in subducting slabs linked to metamorphic dehydration reactions?, *J. Geophys. Res.*, *108*(B1), 2030, doi:10.1029/2001JB001129.

Hart, S. R., and A. Zindler (1986), In search of a bulk-Earth composition, *Chem. Geol.*, *57*, 247–267.

Hilton, D. R., T. P. Fischer, and B. Marty (2002), Noble gases and volatile recycling in subduction zones, in *Noble Gases in Geochemistry and Cosmochemistry*, *Rev. Mineral. Geochem.*, vol. 47, edited by D. Porcelli, C. Ballentine, and R. Weiler, pp. 319–370, Mineral. Soc. of Am., Washington, D. C.

Holland, T. J. B., and R. Powell (1991), A compensated Redlich-Kwong (CORK) equation for volumes and fugacities of $CO_2$ and $H_2O$ in the range of 1 bar to 50 kbar and 100°–1600°, *Contrib. Mineral. Petrol.*, *109*, 265–273.

Holland, T. J. B., and R. Powell (1998), An internally consistent thermodynamic data set for phases of petrological interest, *J. Meteorol. Geol.*, *16*, 309–343.

James, E. R., M. Manga, and T. P. Rose (1999), $CO_2$ degassing in the Oregon Cascades, *Geology*, *27*, 823–826.

Jarrard, R. D. (2003), Subduction fluxes of water, carbon dioxide, chlorine, and potassium, *Geochem. Geophys. Geosyst.*, *4*(5), 8905, doi:10.1029/2002GC000392.

John, T., and V. Schenk (2003), Partial eclogitisation of gabbroic rocks in a late Precambrian subduction zone (Zambia): Prograde metamorphism triggered by fluid infiltration, *Contrib. Mineral Petrol.*, *146*, 174–191.

John, T., E. E. Scherer, K. Hasse, and V. Schenk (2004), Deep global cycling of carbon constrained by the solidus of anhydrous, carbonated eclogite under upper mantle conditions, *Earth Planet. Sci. Lett.*, *227*, 73–85.

Johnson, H. P., and S. W. Semyan (1994), Age variations in the physical properties of oceanic basalts: Implications for crustal formation and evolution, *J. Geophys. Res.*, *99*, 3123–3134.

Johnson, M. C., and T. Plank (1999), Dehydration and melting experiments constrain the fate of subducted sediments, *Geochem. Geophys. Geosyst.*, *1*(1), doi:10.1029/1999GC000014.

Kelemen, P. B., G. M. Yogodzinski, and D. W. Scholl (2003), Along strike variations in lavas of the Aleutian island arc: Implications for the genesis of high Mg# andesite and the continental crust, in *Inside the Subduction Factory*, *Geophys. Monogr. Ser.*, vol. 138, edited by J. Eiler, pp. 23–45, AGU, Washington, D. C.

Keppler, H., M. Wiedenbeck, and S. S. Shcheka (2003), Carbon solubility in olivine and the mode of carbon storage in the Earth's mantle, *Nature*, *424*, 414–416.

Kerrick, D. M. (2001), Present and past non-anthropogenic $CO_2$ degassing from the solid Earth, *Rev. Geophys.*, *39*, 565–585.

Kerrick, D. M. (2002), Serpentinite seduction, *Science*, *298*, 1344–1345.

Kerrick, D. M., and J. A. D. Connolly (1998), Subduction of ophicarbonates and recycling of $CO_2$ and $H_2O$, *Geology*, *26*, 375–378.

Kerrick, D. M., and J. A. D. Connolly (2001a), Metamorphic devolatilization of subducted marine sediments and the transport of volatiles into the Earth's mantle, *Nature*, *411*, 293–296.

Kerrick, D. M., and J. A. D. Connolly (2001b), Metamorphic devolatilization of subducted oceanic basalts: Implications for seismicity, arc magmatism and volatile recycling, *Earth Planet. Sci. Lett.*, *189*, 19–29.

Komiya, T. (2001), Secular change of the composition and temperature of the upper mantle, in *Proceedings of the Extended Abstracts of 4th International Archean Symposium*, *Rec. 2001/37*, edited by K. F. Cassidy et al., pp. 54–56, AGSO-Geosci. Australia, Canberra.

Leeman, W. P., J. F. Lewis, R. C. Evarts, R. M. Conrey, and M. A. Streck (2005), Petrologic constraints on the thermal structure of the Cascades arc, *J. Volcanol. Geotherm. Res.*, *140*, 67–105, doi:10.1016/j.jvolgeores.2004.07.016.

Marty, B., and I. N. Tolstikhin (1998), $CO_2$ fluxes from mid-ocean ridges, arcs and plumes, *Chem. Geol.*, *145*, 233–248.

McHargue, L. R., and P. E. Damon (1991), The global beryllium 10 cycle, *Rev. Geophys.*, *29*, 141–158.

Mishra, O. P., D. Zhao, N. Umino, and A. Hasegawa (2003), Tomography of northeast Japan forearc and its implications for interplate seismic coupling, *Geophys. Res. Lett.*, *30*(16), 1850, doi:10.1029/2003GL017736.

Moore, J. C., and P. Vrolijk (1992), Fluids in accretionary prisms, *Rev. Geophys.*, *30*, 113–135.

Morris, J. D., and F. Tera (1989), $^{10}Be$ and $^{9}Be$ in mineral separates and whole rocks from volcanic arcs: Implications for sediment subduction, *Geochim. Cosmochim. Acta*, *53*, 3197–3206.

Mottl, M. J., C. G. Wheat, P. Fryer, J. Gharib, and J. B. Martin (2004), Chemistry of springs across the Mariana forearc shows progressive devolatilization of the subducting plate, *Geochim. Cosmochim. Acta*, *68*, 4915–4933.

Peacock, S. M. (2001), Are the lower planes of double seismic zones caused by serpentine dehydration in subducting oceanic mantle?, *Geology*, *29*, 299–302.

Peacock, S. M., and K. Wang (1999), Seismic consequences of warm versus cool subduction metamorphism: Examples from southwest and northeast Japan, *Science*, *286*, 937–939.

Peacock, S. M., P. E. van Keken, S. D. Holloway, B. R. Hacker, G. Abers, and R. L. Fergason (2005), Thermal structure of the Costa Rica–Nicaragua subduction zone: Slab metamorphism, seismicity and arc magmatism, *Phys. Earth Planet. Inter.*, *149*, 187–200.

Plank, T., and C. H. Langmuir (1998), The chemical composition of subducting sediment and its consequences for the crust and mantle, *Chem. Geol.*, *145*, 325–394.

Plank, T., et al. (2000), *Proceedings of the Ocean Drilling Program, Initial Reports*, vol. 185, Ocean Drill. Program, College Station, Tex.

Ranero, C. R., and V. Sallarès (2004), Geophysical evidence for alteration of the crust and mantle of the Nazca Plate during bending at the north Chile trench, *Geology*, *32*, 549–552.

Ranero, C. R., J. Phipps Morgan, K. McIntosh, and C. Reichert (2003), Bending-related faulting and mantle serpentinization at the Middle America trench, *Nature*, *425*, 367–373.

Romer, R. L., N. Wawrzenitz, and R. Oberhansli (2003), Anomalous unradiogenic $^{87}Sr/^{86}Sr$ ratios in ultrahigh-pressure crustal carbonates: Evidence for fluid infiltration during deep subduction?, *Terra Nova*, *15*, 330–336.

Rose, E. F., N. Shimizu, G. D. Layne, and T. L. Grove (2001), Melt production beneath Mt. Shasta from boron data in primitive melt inclusions, *Science*, *293*, 281–283.

Rumble, D., J. M. Ferry, T. C. Hoering, and A. J. Boucot (1982), Fluid flow during metamorphism at the Beaver Brook fossil locality, New Hampshire, *Am. J. Sci.*, *282*, 886–919.

Ruepke, L. H., J. Phipps Morgan, M. Hort, and J. A. D. Connolly (2002), Are the regional variations in Central American arc lavas due to differing basaltic versus peridotitic slab fluxing sources?, *Geology*, *30*, 1035–1038.

Sadofsky, S. J., and G. E. Bebout (2001), Paleohydrogeology at 5 to 50 kilometer depths of accretionary prisms: The Franciscan Complex, California, *Geophys. Res. Lett.*, *28*, 2309–2312.

Sano, Y., and S. N. Williams (1996), Fluxes of mantle and subducted carbon along convergent plate boundaries, *Geophys. Res. Lett.*, *23*, 2749–2752.

Scambelluri, M., and P. Philippot (2001), Deep fluids in subduction zones, *Lithos*, *55*(1–4), 213–227.

Shaw, A. M., D. R. Hilton, T. P. Fischer, J. A. Walker, and G. E. Alvarado (2003), Contrasting He-C relationships in Nicaragua and Costa Rica: Insights into C cycling through subduction zones, *Earth Planet. Sci. Lett.*, *214*, 499–513.

Snyder, G., R. Poreda, A. Hunt, and U. Fehn (2001), Regional variations in volatile composition: Isotopic evidence for carbonate recycling in the Central American volcanic arc, *Geochem. Geophys. Geosyst.*, *2*(10), doi:10.1029/2001GC000163.

Staudigel, H., S. Hart, H. Schmincke, and B. Smith (1989), Cretaceous ocean crust at DSDP sites 417–418: Carbon uptake from weathering versus loss by magmatic outgassing, *Geochim. Cosmochim. Acta*, *53*, 3091–3094.

Tatsumi, Y., and S. Eggins (1995), *Subduction Zone Magmatism, Frontiers in Earth Sciences*, Blackwell Sci., Malden, Mass.

van Keken, P. E., B. Kiefer, and S. M. Peacock (2002), High-resolution models of subduction zones: Implications for mineral dehydration reactions and the transport of water into the deep mantle, *Geochem. Geophys. Geosyst.*, *3*(10), 1056, doi:10.1029/2001GC000256.

Vannucchi, P., C. R. Ranero, S. Galeotti, S. M. Straub, D. W. Scholl, and K. McDougall-Ried (2003), Fast rates of subduction erosion along the Costa Rica Pacific margin: Implications for nonsteady rates of crustal recycling at subduction zones, *J. Geophys. Res.*, *108*(B11), 2511, doi:10.1029/2002JB002207.

Varekamp, J. C., and E. Thomas (1998), Volcanic and anthropogenic contributions to global weathering budgets, *J. Geochem. Explor.*, *62*, 149–159.

Wallace, P. J. (2005), Volatiles in subduction zone magmas: Concentrations and fluxes based on melt inclusion and volcanic gas data, *J. Volcanol. Geotherm. Res.*, *140*, 217–240.

Wooley, A. R. (1989), The spatial and temporal distribution of carbonatites, in *Carbonatites: Genesis and Evolution*, edited by K. Bell, pp. 15–37, CRC Press, Boca Raton, Fla.

Zhu, Y., and Y. Ogasawara (2002), Carbon recycled into deep Earth: Evidence from dolomite dissociation in subduction-zone rocks, *Geology*, *30*, 947–950.